JOURNAL OF GEOPHYSICAL RESEARCH, VOL. 94, NO. B4, PAGES 4169–4193, APRIL 10, 1989

M_m: A Variable-Period Mantle Magnitude

EMILE A. OKAL

Department of Geological Sciences, Northwestern University, Evanston, Illinois

JACQUES TALANDIER

Laboratoire de Géophysique, Commissariat à l'Energie Atomique, Papeete, Tahiti, French Polynesia

This paper lays the theoretical groundwork for a variable period mantle magnitude, M_m, based on the measurement of the spectral amplitude $X(\omega)$ of very long period Rayleigh waves. We retain the concept of magnitude by restricting ourselves to single-station measurements, ignoring the focal mechanism and the exact depth of the shallow earthquakes considered. Our measurements are made at a series of periods (in all cases greater than 40 s), and the largest value is retained. This procedure effectively avoids the well-known interference effects leading to saturation of magnitude scales defined at a fixed period. Two corrections are used: a period-dependent distance correction C_D, and a source correction C_S, also period-dependent, compensating for the variation of the excitation of Rayleigh waves with period. Both of these corrections are fully predictable on the basis of standard surface wave excitation and dispersion theory. The result is a formula of the type $M_m = \log_{10} X(\omega) + C_D + C_S + C_0$ in which all coefficients, including the constant C_0 are justifiable on sound theoretical grounds. The analysis of a data set of 256 records from the broadband seismograph at Papeete, Tahiti, the ultra-long period system at Pasadena, and stations of the GEOSCOPE network, shows that the mean error in the estimation of the seismic moment is on the order of 0.1–0.2 units of magnitude, with the standard deviation at each station also on the order of 0.2 units of magnitude. No significant trend with either distance, period, or station can be identified. The method can also be transposed to the time domain, under some simple assumptions which are justifiable theoretically for typical teleseismic distances across the Pacific Basin. Both versions of the method lend themselves well to automation. Thus, by providing a real-time estimate of the seismic moment of distant earthquakes, M_m has considerable potential for tsunami warning purposes. Its concept can easily be extended to Love waves and also to intermediate and deep earthquakes.

1. INTRODUCTION AND BACKGROUND

Magnitudes and Seismic Moments

Ever since it was introduced in the pioneering work of *Richter* [1935], the concept of earthquake magnitude has been used extensively to obtain a rapid evaluation of the size of a seismic event, through the measurement of the amplitude of seismic waves, taken in real time and at a single seismic station. C. F. Richter's original formula, developed empirically for California earthquakes, was later extended to distant earthquakes recorded at Pasadena by *Gutenberg and Richter* [1936], and in the early 1960s, standardized magnitude scales were defined for surface waves at 20 s and body waves at or around 1 s [*Vaněk et al.*, 1962]. For about 30 years, magnitudes of one scale or another were the only available measurements of the size of earthquakes. In all cases, magnitudes were directly related to the logarithm (base 10) of the recorded amplitude of ground motion.

The situation evolved significantly in the 1960s when various combinations of systems of forces were investigated as physical descriptions of earthquake sources. *Aki* [1966] showed that the physical characterization of most earthquake sources was a double couple quantified by its seismic moment M_0 having dimensions of energy. Because of the linearity of all the physical laws involved, the excitation of all seismic waves by a point source double-couple is proportional to M_0. As such, in the absence of any additional effects, the relationship between M_0 and any magnitude M would be expected to take the form

$$M = \log_{10} M_0 + \text{const} \tag{1}$$

the theoretical value of the slope being exactly 1.

However, a well-known problem of any of the classical magnitude scales is their saturation, as the true size of the seismic source, M_0, keeps growing. This has been explained in detail by *Aki* [1967, 1972] and later *Geller* [1976], as due to the destructive interference resulting from the spatiotemporal extent of the seismic source. In simple terms, as an earthquake grows in size, it reaches a point when the actual duration of the source process becomes comparable to, if not longer than, the period ($T = 20$ s for M_s) at which the magnitude is measured, leading to variation in the initial phase of the wave during the rupture process, and eventually to destructive interference.

In *Geller*'s [1976] model, interference effects bringing nonlinearity between $\log_{10} M_0$ and M_s start at about $M_0 = 4 \times 10^{25}$ dyn-cm. Between this value and $M_0 = 5 \times 10^{27}$ dyn-cm, a slope of 2/3 between M_s and

Paper number 88JB04010.
0148-1227/89/88JB-04010$05.00

$\log_{10} M_0$ is predicted. Beyond $M_0 = 1.5 \times 10^{28}$ dyn-cm, full saturation is predicted. Thus earthquakes with measured M_s values of 8.0–8.3 can have seismic moments differing by a factor of 1000. Obviously, this makes the use of M_s in interpreting the "size" of gigantic earthquakes worthless, if not outright dangerous, for example when assessing their tsunamigenic potential.

Purpose of This Study

Because it relies on a real-time measurement of the seismic signals recorded at a single station, the magnitude concept remains a simple and powerful tool of observational seismology. The purpose of the present paper is thus to explore the possibility of developing a magnitude scale, M_m, allowing the retrieval of the seismic moment within an acceptable range of precision, while keeping the basic philosophy of the magnitude concept, i.e., the use of a single station, and the rapidity of the measurement.

The rationale behind this philosophy derives from the importance of measuring M_0 in the context of tsunami warning. While it has been known for a long time that the static value of the seismic moment is a key factor in tsunami genesis, we have recently shown that the influence on tsunami excitation of focal mechanism, and to a large extent of depth in the 0–75 km range, is actually minimal [*Okal*, 1988]. Thus it may be futile to use the precious time separating the arrivals of surface and tsunami waves for the purpose of refining depth estimates or of obtaining an exact focal geometry. This is especially true when the epicentral distance is short, as can be the case between the Aleutian Islands and Alaska or between the Tonga arc and Tahiti. In particular, it must be borne in mind that most reliable moment tensor inversions still require the acquisition of seismic data at a large number of stations; for such short distances there may not be sufficient time to wait for the arrival of even the first passage of Rayleigh waves at more distant seismic stations. Therefore, even in the days of supposedly instant worldwide satellite telecommunications, the possibility of determining a seismic moment from the records of a single seismic observatory remains very valuable. One of our goals will be to make sure that the concept of M_m remains valid at relatively short distances (see section 5).

An additional goal in this study will be to provide an analytic expression for the magnitude scale derived from theoretical grounds, so that all constants in the eventual formula for M_m can be fully predicted from theoretical models of earthquake sources and seismic propagation. We will relate the mantle magnitude M_m to the seismic moment through:

$$M_m = \log_{10} M_0 - 20 \qquad (2)$$

where M_0 is measured in dyn-cm. The choice of the constant 20 in (2) is of course arbitrary; however, it has the advantage of keeping the values of M_m within a practical, usual, range; for example, an earthquake of moment 10^{28} dyn-cm has an M_m of 8.0 . We will derive and test ways of measuring an estimate of M_m in real time from the records of a single seismic observatory.

In order to avoid the saturation phenomena described above, it is clear that we need to move to very long periods. We will make the measurement wherever in the frequency domain the signal has sufficient energy. Thus emerges the concept of a variable-period magnitude. In practice, we will always seek to measure M_m on the flat portion of the source spectrum, i.e., at a frequency less than the corner frequency ω_{CF} of the source.

What makes this approach possible is the development, in recent years, of a new generation of broadband seismometers [*Wieland and Streckeisen*, 1982] with large dynamic range, which allow the reliable recording of the seismic signal without the all too frequent problems of nonlinearity and saturation (clipping) which used to plague the recording of the first passage of surface waves from truly large events on older instruments. We refer to *Monfret and Romanowicz* [1986] for a discussion of the theoretical advantages of using first passages; in addition, in the context of tsunami warning, it is crucial to obtain a measurement as rapidly as possible.

However, we want to emphasize that a number of stations did operate reliable low-gain ultra-long-period or broadband instruments, as far back as the 1960s. Notable among such systems is the Pasadena ultra-long-period vertical ("number 33") seismometer [*Gilman*, 1960; *Brune and King*, 1967] and the LDG broadband operated at Papeete, Tahiti since 1972. Records from these instruments will, together with the recent GEOSCOPE digital data, provide the experimental backbone of the present study. A typical example, shown on Figure 1, emphasizes the prominence of long-period energy in the 200–s range; it is safe to say that had such records been available at the time, the founding fathers of magnitude scales would probably have attempted to quantify the earthquake source from information at the lower end of the frequency spectrum, rather than around 20 s. The development of M_m can then be regarded as a modernization of the concept of magnitude in view of recent developments in instrumentation.

Finally, in this study we restrict ourselves to shallow earthquakes ($h < 75$ km). Our experience shows that it is generally possible from a single seismic observatory to ascertain immediately the general character (shallow, intermediate, deep) of a teleseismic event. In section 6 we propose to extend the concept of M_m to intermediate and deep earthquakes; these events, however, do not carry substantial tsunami risk, and thus some of the motivation for the fast retrieval of their seismic moment disappears.

2. Previous Work Along Similar Lines

Brune and King [1967]

A similar attempt at quantifying earthquakes from the very long period characteristics of their seismic source can be traced back to *Brune and King* [1967], who investigated the spectral amplitude of 100-s Rayleigh waves. However, these authors were working at a fixed period, and any such magnitude M_{100} would still be expected to saturate for sufficiently large earthquakes. Indeed, nonlinear effects should yield a 2/3 slope between M_{100} and

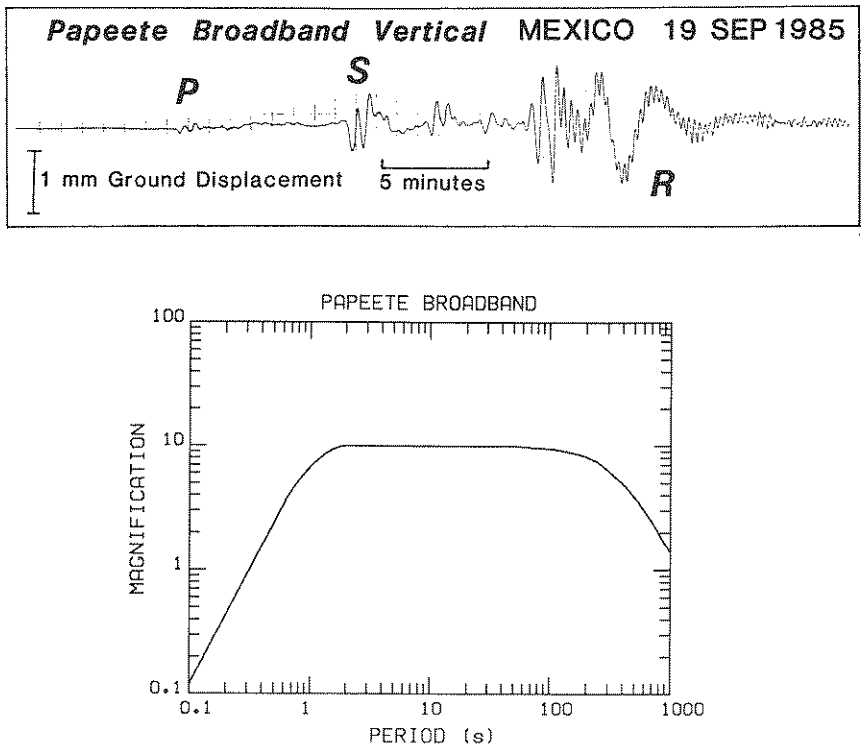

Fig. 1. (Top) Example of broadband record at PPT. Note the prominent mantle Rayleigh waves. (Bottom) Frequency response of the broadband system at PPT.

$\log_{10} M_0$ beyond 10^{28} dyn-cm, precisely in the range of great earthquakes with significant tsunamigenic potential. This limitation is partly responsible for the "S curve" behavior of M_{100} versus M_s, as reported for example on *Brune and King*'s [1967] Figure 3.

In turn, *Brune and Engen* [1969] proposed a mantle wave magnitude, based empirically on this very figure; however, they did not provide a simple formula for the exact expression of their magnitude scale but rather gave two plots, one in the time domain for Rayleigh waves and one in the frequency domain for Love waves, relating amplitudes at 100 s to seismic moment and to the proposed 100-s magnitude. In addition, it is noteworthy that they characterized the 1964 Alaskan earthquake as larger than the 1960 Chilean event, whereas most ultra-long-period studies [*Kanamori*, 1970; *Kanamori and Cipar*, 1974; *Geller*, 1977; *Cifuentes and Silver*, 1989] indicate that it was at least 3 times smaller in moment. This is a direct illustration of the failure of any magnitude computed at a fixed period for sufficiently large seismic sources, as noted also by *Purcaru and Berckhemer* [1982].

Kanamori's [1977] *Moment Magnitude* M_w

In order to alleviate some of the difficulties inherent in saturation, *Kanamori* [1977] proposed the concept of a moment magnitude (which he also called "energy magnitude"):

$$M_w = \frac{2}{3} (\log_{10} M_0 - 16.1) \qquad (3)$$

In this approach, M_w is actually computed from M_0, once the latter has been obtained through moment tensor inversion or similar techniques. Specifically, Kanamori was seeking to extend M_s beyond its point of total saturation and thus to provide continuity with large, but not gigantic, earthquakes (typically in the range 10^{27} dyn-cm, where interference effects are significant, but full saturation is not yet attained). Thus, he introduced an a priori slope of 2/3 in the definition of M_w. In doing so, he also extended *Gutenberg*'s [1956] relation between the total seismic energy released and magnitude, $\log_{10} E = 1.5\, M + 11.8$, which, in the framework of modern source theory, is now understood to hold only in the same range of magnitudes. Therefore one can predict that while M_w will behave like M_s for these large, "interesting" earthquakes, a significant discrepancy will occur for smaller events, for which M_s should be smaller than M_w.

Along similar lines, *Purcaru and Berckhemer* [1978] introduced their energy magnitude, M_E, which differs from M_w in that an allowance is made for a variable stress drop $\Delta\sigma$.

Ekström and Dziewonski's [1988] $\overline{M_s}$ *: An Improved* M_w

The observation of an M_s:M_w discrepancy for small events, and the resulting systematic bias in the estimate of seismic moment release if (3) is used backward to compute M_0 from M_s, prompted *Ekström and Dziewonski* [1988] to propose a magnitude $\overline{M_s}$ combining M_w behavior for large earthquakes while remaining comparable to M_s for smaller ones and with a gradual transition in between. Whereas $\overline{M_s}$ is clearly superior to M_w, this

approach does not differ substantially from *Kanamori*'s [1977], in that it consists fundamentally of recasting a measurement of M_0 (obtained from a full moment tensor inversion) into the more popular range of magnitude values; or conversely of using 20-s M_s measurements predating digital seismology to obtain an estimate of moment release.

Williams' [1979] AR Method

An interesting attempt at recovering M_0 in real time can be found in *Williams* [1979]. It consists of measuring the so-called *AR* parameter, which amounts to integrating the square of the displacement during the first passage of Love and Rayleigh waves. Basically, Williams follows our philosophy of using the records of a single long-period station. However, because she limits herself to WWSSN records dominated mostly by 20- to 50-s energy, she must use two different formulæ (with slopes close to 1.0 and 1.5) to reproduce the initiation of saturation around $M_0 = 7 \times 10^{27}$ dyn-cm. By the same token, her method would fail when total saturation is reached: it is noteworthy that the largest moment in her data set is only 1.5×10^{28} dyn-cm.

Finally, a preliminary version of the present study was published by *Okal and Talandier* [1987] and *Talandier et al.* [1987]. In the present paper we give the full theoretical treatment justifying the expressions of M_m and present an extensive data set of more than 250 measurements worldwide, fully upholding the validity of the endeavor and its reliability.

3. THEORY

Since we seek a very long period measurement of the seismic moment of an earthquake, we will base the development of M_m on the theory of the excitation and propagation of Rayleigh waves. We adopt the formalism and notation of *Kanamori and Stewart* [1976]. The spectral amplitude at angular frequency ω of a Rayleigh wave recorded at a distance Δ from an earthquake can be written as

$$X(\omega) = a\sqrt{(\pi/2)}\left[e^{-\omega a \Delta/2UQ} / \sqrt{\sin\Delta}\right] \times \left[\frac{1}{U}\left| s_R K_0 l^{-1/2} - p_R K_2 l^{3/2} - i q_R K_1 l^{1/2} \right| M_0\right] \quad (4)$$

In this equation we have separated terms due to propagation (on the first line) and to excitation (on the second line). The effect of propagation consists of the geometrical spreading $1/\sqrt{\sin\Delta}$ and of the anelastic attenuation along the path $a\Delta$. The excitation terms include the seismic moment M_0 and the combination of the excitation coefficients K_i (depending on depth and frequency), and of the trigonometric terms p_R, q_R, s_R describing the geometry of the faulting in relation to the azimuth of the station. We refer to *Kanamori and Cipar* [1974] and *Kanamori and Stewart* [1976] for the exact expressions of these coefficients; finally, a is the Earth's radius, l the angular order of the equivalent normal mode, and U the group velocity of the wave.

Conversely, the seismic moment M_0 (or the mantle magnitude M_m) of the event can be retrieved from the spectral amplitude through

$$\log_{10} M_0 = M_m + 20 = \log_{10} X(\omega) + C_D + C_S + C \quad (5)$$

where C_D is a distance correction related to the first bracket in (4), C_S is a source correction related to the second bracket, and $C = \log_{10}(\sqrt{(2/\pi)}/a)$ is a constant. $C = -3.90$ if a is in kilometers.

Distance Correction

The distance correction is simply

$$C_D = \frac{1}{2}\log_{10}\sin\Delta + (\log_{10} e)\,\frac{\omega a \Delta}{2UQ} \quad (6)$$

These terms are obviously independent of focal mechanism and depth. In order to reflect the possible influence of lateral heterogeneity on U and Q, we use a model of the Earth regionalized into seven tectonic regions, using a $10° \times 10°$ grid (Figure 2). This regionalization generally follows the previous work of *Okal* [1977], *Jordan* [1981], and, for the oceanic areas, *Mitchell and Yu* [1980]. The seven regions considered are four oceanic age bands (0–20 Ma; 20–50 Ma; 50–100 Ma; older than 100 Ma); two continental regions, shields and mountains (which we can define as active in the past 500 m.y.); and finally a "trench and subduction zone" area.

In view of the recent results in seismic tomography [e.g., *Woodhouse and Dziewonski*, 1984] showing some decoupling of the pattern of deep heterogeneity from that of the obvious tectonic features at the surface, the accuracy of this regionalization at very long periods can be doubted. However, as expected from (6) and discussed later in section 5, when the period becomes very large, the attenuation correction decreases to the point where the effect of regionalization becomes minimal and the issue insignificant.

Regionalized values of U and Q were obtained based on the work of *Canas and Mitchell* [1978], *Mitchell and Yu* [1980], *Nakanishi* [1981], and *Hwang and Mitchell* [1987]. Table 1 lists all the values of U and Q used in the computation of C_D. Once an epicenter has been obtained, the path under study is split into segments belonging to the various regions, and their contributions to the second term in C_D are simply added.

Source Correction

This correction

$$C_S = -\log_{10}\left|\left(s_R\frac{K_0}{\sqrt{l}} - p_R K_2 l^{3/2} - i\, q_R K_1 l^{1/2}\right) / U\right| \quad (7)$$

is expected to be a priori dependent on focal mechanism and depth, through the coefficients K_i. In keeping with the magnitude concept, and the discussion in the introductory section, we assume that these parameters are unknown and proceed to compute C_S for an average excitation, representative of an average focal mechanism and station orientation and of an average depth in the range 10–75 km.

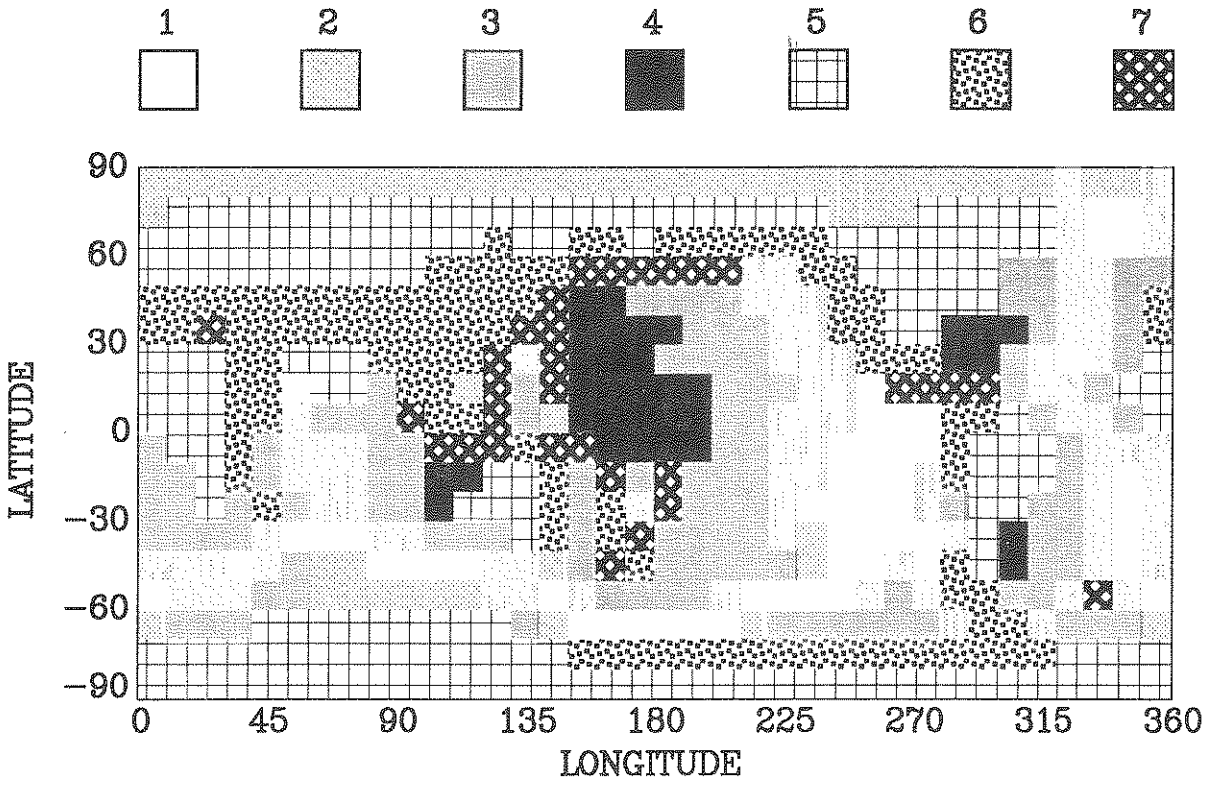

Fig. 2. Tectonic regionalization used in the computation of the distance correction C_D. The various shading patterns refer to oceans (1, less than 20 Ma; 2, 20–50 Ma; 3, 50–100 Ma; 4, older than 100 Ma); continents (5, shields; 6, tectonic regions); and trenches (7). See Table 1 for corresponding values of U and Q.

Whether or not one can neglect the influence of focal mechanism and depth and still obtain a reliable estimate of the seismic moment M_0 will eventually make or break the concept of M_m, the variable-period mantle magnitude, as a viable measurement of the "size" of the earthquake. As discussed more in detail in section 5, we believe that our results are extremely encouraging in this respect.

For our purpose, we define the excitation of a Rayleigh

TABLE 1. Regionalized Dispersion and Attenuation Models Used in Computing Distance Correction

	Region 1 0–20 Ma		Region 2 20–50 Ma		Region 3 50–100 Ma		Region 4 > 100 Ma		Region 5 Shields		Region 6 Mountains		Region 7 Trenches	
T, s	U, km/s	Q	U, km/s	Q	U, km/s	Q	U, km/s	Q	U, km/s	Q	U, km/s	Q	U, km/s	Q
35	3.845	158	4.005	168	4.046	200	4.013	251	3.455	236	2.950	98	2.880	96
38	3.836	152	3.995	162	4.061	191	4.040	234	3.536	220	3.070	95	2.900	90
42	3.819	147	3.976	155	4.063	181	4.064	217	3.634	204	3.170	92	2.920	85
46	3.799	143	3.953	150	4.055	173	4.074	204	3.722	192	3.250	90	2.940	82
51	3.772	139	3.927	145	4.043	166	4.073	191	3.818	181	3.300	92	2.960	79
56	3.746	136	3.899	140	4.023	159	4.062	183	3.858	177	3.380	94	2.980	78
63	3.714	133	3.863	136	3.992	153	4.037	175	3.899	181	3.520	96	3.000	79
70	3.690	131	3.831	134	3.958	149	4.007	169	3.920	179	3.560	98	3.040	80
78	3.670	129	3.799	132	3.919	145	3.972	166	3.936	192	3.620	100	3.070	81
87	3.657	129	3.770	131	3.879	143	3.934	165	3.954	212	3.690	103	3.100	82
90	3.649	130	3.743	132	3.836	142	3.893	166	3.952	251	3.710	106	3.130	84
111	3.642	133	3.718	134	3.794	144	3.850	170	3.928	260	3.700	109	3.170	87
127	3.632	138	3.694	140	3.753	148	3.806	177	3.896	295	3.680	112	3.218	92
145	3.617	146	3.671	149	3.715	155	3.761	188	3.854	333	3.700	116	3.419	99
167	3.590	159	3.643	161	3.673	168	3.710	203	3.797	280	3.780	120	3.515	108
193	3.554	177	3.611	180	3.631	187	3.657	222	3.743	250	3.580	125	3.623	119
223	3.524	201	3.586	204	3.601	209	3.617	245	3.666	283	3.550	130	3.526	131
259	3.541	231	3.606	234	3.620	239	3.628	272	3.645	312	3.470	155	3.475	149
300	3.669	262	3.727	266	3.742	271	3.745	297	3.706	345	3.610	200	3.699	170

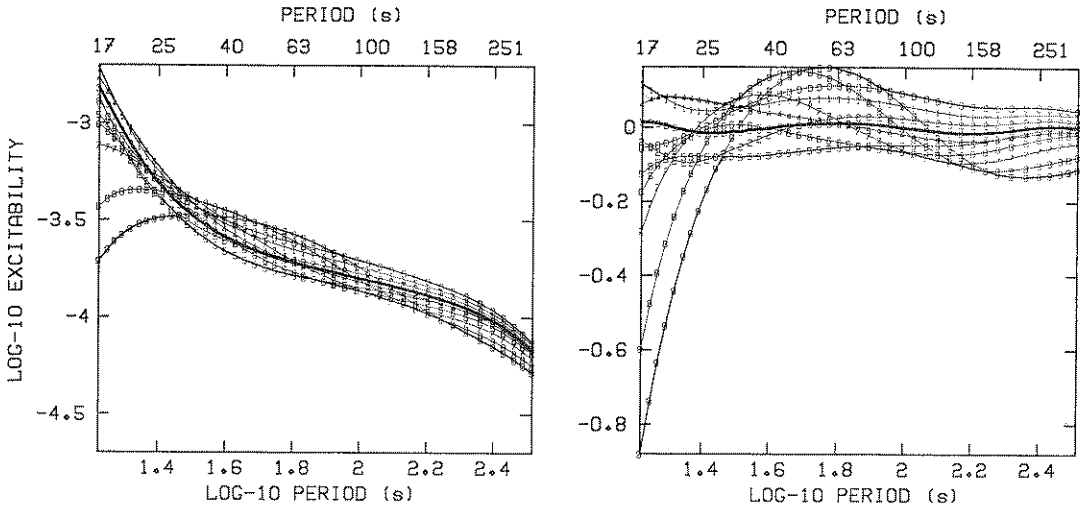

Fig. 3. (Left) Logarithmic average excitability as defined by (9) plotted as a function of period and depth. The various symbols (from 0 to 9) refer to 10 sampling depths between 10 and 75 km. The thicker trace corresponds to $h = 20$ km, which is retained for the computation of C_S. (Right) Same as left, after the correction C_S given by (10) has been applied. Note that beyond $T = 35$ s, the maximum error remains at most ±0.15 orders of magnitude.

wave of angular frequency ω by an earthquake at depth h and in a particular geometry as

$$E(\phi_f, \delta, \lambda; \phi_s; h; \omega) = \left| (s_R K_0 l^{-1/2} - p_R K_2 l^{3/2} - i\, q_R K_1 l^{1/2}) / U \right| \quad (8)$$

and the "logarithmic average excitability" of the wave for a given depth and frequency as

$$L_{av} = \log_{10} E_{av}(h, \omega) = \log_{10} \left[\frac{1}{N} \sum E(\phi_f, \delta, \lambda; \phi_s; h; \omega) \right] \quad (9)$$

i.e., the logarithm of the average of E, taken over a large number N of combinations of the fault dip δ, slip λ, strike ϕ_f, and station azimuth ϕ_s. In practice, we used the PREM model [*Dziewonski and Anderson*, 1981] to compute the coefficients K_i at 10 depths ranging from 10 to 75 km and 44 periods from 16 to 300 s. We then averaged over $N = 6480$ geometries. We want to point out that this definition is somewhat different from the value of E_{av} proposed by *Okal and Talandier* [1987]. In that preliminary work we had averaged the logarithms, thus placing extreme emphasis on nearly nodal geometries (when these exist) and hence biasing C_S toward higher values. Here we average the excitations themselves before taking the logarithm in (9).

At any depth the use of an average excitation instead of the exact value of E results in a substantial systematic error only in the case of an event with a "pure" focal mechanism (either purely horizontal or purely vertical slip on a perfectly vertical fault plane) and a station at the node of the radiation pattern, for which the expected excitation is identically zero. For other mechanisms, and in particular for the thrust and normal faults typical of the great majority of the truly gigantic events bearing substantial tsunami risk, it is usually possible to find a period at which the sharpness of the nodes of the radiation pattern is considerably reduced; under these conditions the systematic error on $\log_{10} E$ usually remains less than ± 0.2 units of magnitude.

Results are shown in Figure 3, with the coefficients K_i expressed in units of 10^{-27} dyn^{-1} and U in km/s. It is clear that at periods greater than 40 s, the dependence of L_{av} on h is minimal and that the logarithmic average excitability at 20 km is an adequate depth average, except for shorter periods. We thus restrict ourselves from now on to periods $T \geq 40$ s and further smooth L_{av}(20 km) by a cubic spline. This leads to the following expression for C_S:

$$C_S = 1.6163\ \theta^3 - 0.83322\ \theta^2 + 0.42861\ \theta + 3.7411 \quad (10)$$

where $\theta = \log_{10} T - 1.8209$. Figure 3 (right) shows that the deviation of L_{av} due to depth-averaging is at most ±0.15 orders of magnitude between the depths of 10 and 75 km. The range of variation of C_S itself is from 3.590 at $T = 40$ s to 4.120 at $T = 300$ s. In the above formulæ, we use practical seismological units, i.e., T is in seconds, a in kilometers, U in km/s, K_i in 10^{-27} dyn^{-1}. By combining the previous equations, we obtain

$$M_m = \log_{10} X(\omega) + C_D + C_S + C_0 \quad (11)$$

with C_D computed according to (6), C_S given by (10), $C_0 = -0.90$, and $X(\omega)$ measured in μm-s, following the practice, common in magnitude studies, of measuring ground displacements in microns.

From Theory to Application: How to Avoid Source Finiteness Effects

The above theory was developed for a point source, both in the time and space domains. Before we can apply our results to real data, we must devise a strategy

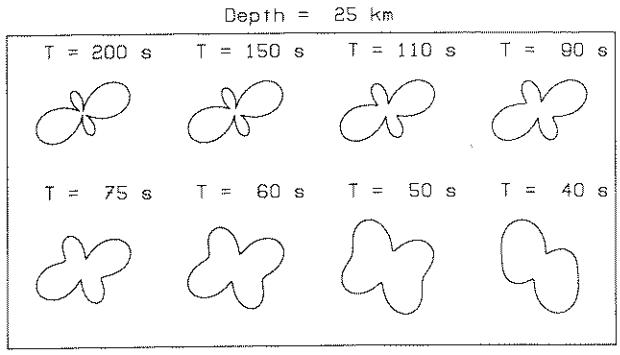

Fig. 4. Variation of the azimuthal radiation pattern of the spectral amplitude $X(\omega)$ as a function of period, in the geometry $\phi = 13°$; $\delta = 71°$; $\lambda = 36°$. Note the disappearance of secondary nodes at higher frequencies [after *Okal and Talandier*, 1987].

for choosing the frequency at which the measurement will be made and in particular ensuring that this frequency is indeed on the flat portion of the spectrum, below the corner frequency. The simplest idea in this respect is to use many frequencies, say all periods between 40 and 300 s, and retain the largest computed value of M_m. The rationale behind this procedure is that the interference due to finiteness of the source is always destructive and thus biases M_m toward lower values. We will see that in general, this algorithm does indeed retain a measurement taken at a very long period.

Another possibility would be to always measure M_m at some fixed, but very long period (e.g., 300 s). The problem with this approach is twofold: first, there may not always be an adequate signal-to-noise ratio especially for smaller events in the 10^{26} dyn-cm range, and we may actually be measuring noise; second, and more importantly, a variable period helps guard against the possibility of a station sitting in a node of Rayleigh radiation at a particular period. Obviously, in the case of a "pure" mechanism, the azimuths of the nodes are frequency independent; however, as shown on Figure 4, the shape of radiation patterns can strongly depend on frequency for mechanisms involving nonvertical faults and/or oblique slip. Then a change of reference period can literally move the station out of a node. Thus we prefer to compute M_m at many frequencies and keep the largest value.

If, on the other hand, our measurements were taken in a portion of the spectrum beyond the first corner frequency due to finite length of rupture, ω_{CF}, one would have to add to (4) an additional factor [sinc $(\omega\tau_s/2)$], where τ_s is the duration of rupture. Conversely, beyond ω_{CF}, one would expect an additional correction to (11)

$$C_{CF} = \log_{10} (\pi\tau_s / T) \qquad (12)$$

since the sine function in "sinc" approaches 1 beyond ω_{CF}.

If τ_s scales with $M_0^{1/3}$, one predicts a relationship of the form $M_0 \propto [\omega X(\omega)]^{3/2}$. Conversely, M_m computed from (11) would actually vary as $(2/3) \log_{10} M_0$. If τ_s can be taken as constant, one predicts $M_0 \propto [\omega X(\omega)]$, and M_m computed from (11) should be off by a term $[C_1 - \log_{10} T]$. This constant behavior of τ_s would be suggested to some extent by the parameters of moderate to large earthquakes obtained from the Harvard centroid moment tensor inversions [*Dziewonski et al.*, 1983*a,b,c*, 1984*a,b*, 1985*a,b,c,d*, 1986*a,b,c*, 1987*a,b,c,d,e,f,g*, 1988 *a,b,c,d,e*]. We refer to *Okal and Talandier* [1987] for a full discussion of these effects and for the exact formulæ expected under these conditions.

An important series of tests, which we will conduct in the section 5, is to verify that the best fitting slope between published values of $\log_{10} M_0$ and M_m computed from (11) is indeed close to 1. This will be the ultimate test to ascertain that we remain beyond the corner frequency of the event and are not affected by the saturation effects.

Should we find a slope of 3/2 (or simply significantly greater than 1) between $\log_{10} M_0$ and M_m, we would conclude that we have failed to avoid saturation. Similarly, should we find a strong variation in the quality of our fit with period, we could still be contaminated by finiteness with the earthquake data set following a model with constant τ_s.

4. APPLICATION TO DATA

Our data for this study consist of three sets: (1) records obtained at the broadband station operated at Papeete, Tahiti (PPT), since 1972; (2) records obtained on the ultra-long-period vertical instrument at Pasadena, California (PAS); and (3) records from the GEOSCOPE network.

Papeete Records

As shown on Figure 1, the response of this system is flat in displacement from 1 s to 150 s and decreases by a factor $\sqrt{2}$ at 300 s. We concentrate here on a data set of 45 earthquakes, listed in Table 2, and having published moments between 7.6×10^{25} and 1.8×10^{28} dyn-cm. Their locations and focal mechanisms are shown on Figure 5.

For each event, we Fourier-transformed a 4096-point time series (with digital sampling rate 0.2 s) and at each Fourier period $T \geq 50$ s obtained the spectral amplitude $X(\omega)$ after removal of the instrument response; we then applied the corrections (6) and (10) and computed a value of M_m using (11). We list in Table 2 only the largest value, and the period at which it is obtained, but keep all measurements as a permanent data set.

Pasadena Records

This system (commonly called ULP33) has been described by *Gilman* [1960] and its response is given by *Okal and Geller* [1979]. This is not a broadband system but rather a classical electromagnetic seismograph system with a filtered galvanometer, resulting in an overall maximum response peaked at 145 s. We selected all available records of events with published moments greater than 10^{26} dyn-cm from 1970 to 1986. Unfortunately, the instrument was not operating between April 1983 and the

TABLE 2. Papeete Data Set

Event	Station	Passage	Δ	M_m^{pub}	M_m	T	r	M_c	r_c
1973 06 17	PPT	1	84.68	7.85	8.20	273.0	0.35	7.85	0.00
1974 10 03	PPT	1	69.18	8.26	8.13	164.0	-0.13	8.17	-0.09
1977 04 21	PPT	1	48.74	7.08	7.08	63.0	0.00	7.24	0.16
1977 06 22	PPT	1	25.24	8.15	8.23	117.0	0.08	8.02	-0.13
1978 03 23	PPT	1	83.95	7.43	7.30	273.0	-0.13	7.25	-0.18
1978 03 24	PPT	1	83.32	7.36	7.29	205.0	-0.07	7.09	-0.27
1978 06 12	PPT	1	84.80	7.53	7.51	273.0	-0.02	7.43	-0.10
1978 11 29	PPT	1	62.01	7.72	7.27	205.0	-0.45	7.59	-0.13
1979 02 16	PPT	1	73.03	6.79	6.68	82.0	-0.11	6.47	-0.32
1979 02 28	PPT	1	78.34	7.27	7.15	273.0	-0.12	7.02	-0.25
1979 03 14	PPT	1	59.17	7.24	7.35	205.0	0.11	7.30	0.06
1979 10 12	PPT	1	46.82	7.00	7.00	164.0	0.00	6.96	-0.04
1980 07 08	PPT	1	42.78	7.29	7.52	205.0	0.23	7.26	-0.03
1980 07 17	PPT	1	43.19	7.90	7.95	205.0	0.05	7.67	-0.23
1981 07 06	PPT	1	36.59	7.41	7.22	82.0	-0.19	7.47	0.06
1981 07 15	PPT	1	40.79	6.76	7.01	205.0	0.25	6.72	-0.04
1981 09 01	PPT	1	22.72	7.29	7.28	273.0	-0.01	7.40	0.11
1981 10 25	PPT	1	58.68	6.85	7.12	273.0	0.27	6.95	0.10
1982 06 07 A	PPT	1	61.04	6.46	6.52	205.0	0.06	6.70	0.24
1982 06 07 B	PPT	1	60.84	6.43	6.71	273.0	0.28	6.73	0.30
1982 08 05	PPT	1	43.16	6.51	6.96	273.0	0.45	6.63	0.12
1982 12 19	PPT	1	25.39	7.30	7.47	273.0	0.17	7.36	0.06
1983 05 26	PPT	1	87.84	7.66	7.99	164.0	0.33	7.57	-0.09
1983 10 04	PPT	1	72.74	7.53	7.55	205.0	0.02	7.37	-0.16
1984 02 07	PPT	1	48.97	7.40	7.55	59.0	0.15	7.50	0.10
1984 03 24	PPT	1	83.67	6.80	6.93	273.0	0.13	6.72	-0.08
1985 03 03	PPT	1	70.32	8.01	7.89	164.0	-0.12	7.69	-0.32
1985 04 09	PPT	1	70.53	6.70	6.87	55.0	0.17	6.59	-0.11
1985 09 19	PPT	1	58.40	8.04	7.94	205.0	-0.10	7.81	-0.23
1985 09 21	PPT	1	58.87	7.40	7.44	205.0	0.04	7.30	-0.10
1985 11 28 A	PPT	1	42.58	6.48	7.01	273.0	0.53	6.60	0.12
1985 11 28 B	PPT	1	42.64	6.56	6.75	82.0	0.19	6.80	0.24
1985 12 21	PPT	1	42.33	6.76	6.98	205.0	0.22	6.71	-0.05
1986 04 30	PPT	1	58.18	6.49	6.64	205.0	0.15	6.51	0.02
1986 05 07	PPT	1	72.38	8.02	8.13	205.0	0.11	7.85	-0.17
1986 10 20	PPT	1	27.08	7.95	7.83	63.0	-0.12	7.69	-0.26
1987 02 08	PPT	1	62.16	7.05	7.30	117.0	0.25	7.04	-0.01
1987 03 05	PPT	1	73.50	7.39	7.51	51.0	0.12	7.26	-0.13
1987 03 06	PPT	1	75.33	6.80	6.87	137.0	0.07	6.57	-0.23
1987 06 27	PPT	1	72.44	5.92	6.10	59.0	0.18	6.16	0.24
1987 07 06	PPT	1	41.06	5.98	6.45	117.0	0.47	6.03	0.05
1987 08 08	PPT	1	74.88	6.90	7.12	68.0	0.22	6.72	-0.18
1987 09 03	PPT	1	55.90	7.15	6.88	205.0	-0.27	7.35	0.20
1987 09 28 A	PPT	1	40.17	6.28	6.40	137.0	0.12	6.16	-0.12
1987 09 28 B	PPT	1	40.15	5.88	5.98	164.0	0.10	5.72	-0.16

fall of 1986, which prevents a direct comparison with PPT and GEOSCOPE records, especially for the large earthquakes of 1985 and 1986. We also had to eliminate a number of records featuring gross nonlinearity in the response of the instrument; (e.g., October 11, 1975; March 14, 1979). Records were hand-digitized at a sampling rate of 1 s, and the analysis proceeded as for the PPT records. However, in view of the faster falloff of the response curve at long periods, we take our measurements only in the range 50–250 s. We include in the PAS data set records of multiple passages of Rayleigh waves for some of the largest events involved. For such records we restrict our measurements to $T \geq 75$ s for R_2 and $T \geq 100$ s for R_3 and R_4. The full data set comprises 42 records from 31 earthquakes, whose locations and mechanisms are shown on Figure 6. Results are listed in Table 3.

GEOSCOPE records

We refer to *Romanowicz et al.* [1984] for a description of the GEOSCOPE network, including its frequency response. In this study we targeted all available GEOSCOPE records from shallow earthquakes of moment $M_0 \geq 10^{26}$ dyn-cm; however, we eliminated records with poor signal-to-noise ratios, records early in the history of the network for which high magnification led to digital clipping and/or nonlinearity, and records from the station MBO (M'Bour, Senegal) for which the magnification level is in doubt. Table 4 lists all records in the GEOSCOPE study. Data processing was analogous to that for PPT. However, in view of the time sampling of the VLP channel ($\delta t = 10$ s), we take measurements only at periods $T \geq 64$ s. As in the case of PAS, we include a number of second passages of Rayleigh waves, for which

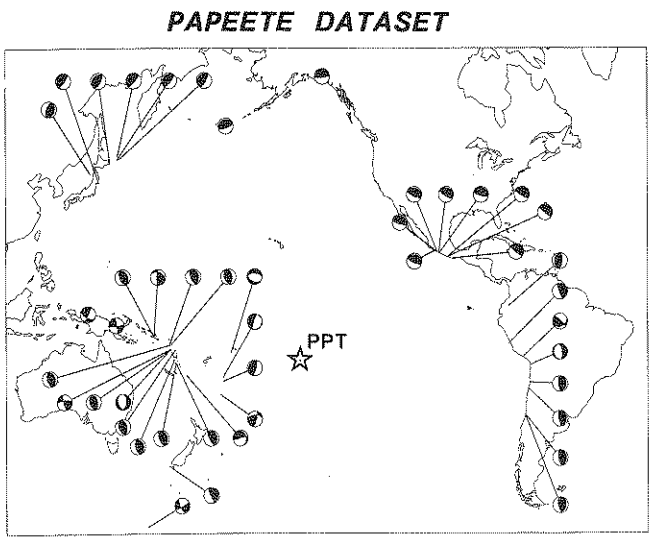

Fig. 5. Map of the epicenters and focal mechanisms for the Papeete data set.

we restrict measurements to $T \geq 75$ s. We also include in the data set all multiple passages, up to and including R_4, in the case of the Aleutian earthquake of May 7, 1986, our purpose being to test any systematic bias of the measured M_m as a function of distance; we do not include similar records for the preceding large events (e.g., the Chilean and Mexican 1985 earthquakes), since at the time the network was not yet fully developed. As explained below, measurements for R_5 deteriorate substantially, suggesting that the signal-to-noise ratio is by then too low for a significant measurement. We list the corresponding values at the end of the data table but do not use R_5 values in our statistical evaluations. The full data set comprises 169 records (178 with R_5) from 41 earthquakes, whose location and mechanisms are shown on Figure 7.

In studying the performance of the magnitude scale M_m, we consider separately the three data sets described above and also regroup them as a single data set comprising all 256 measurements. Thus we will commonly refer to four data sets.

Published Moments and Focal Mechanisms

We take most of our published moments from the Harvard moment tensor inversion solutions [*Dziewonski et al.*, 1983*a,b,c*, 1984*a,b*, 1985*a,b,c,d*, 1986*a,b,c*, 1987*a,b,c,d,e,f,g*, 1988*a,b,c,d,e*]. A variety of sources are used for events predating 1977. We occasionally use our own solutions for earthquakes which we have studied in detail. Table 5 lists all pertinent epicentral data. In Tables 2, 3, and 4, the published moments are reported through M_m^{pub}, obtained by applying (2) to the published value of the moment, as listed in Table 5.

Finally, we note that the largest event analyzed is the 1977 Indonesian earthquake ($M_0 = 3.6 \times 10^{28}$ dyn-cm). Obviously, the systematic study of the performance of the method for truly gigantic events (in the 10^{29} to 10^{30} dyn-cm range) would be a fundamental test of the method. However, such events have not occurred since 1965. Our purpose in the present paper is to test the concept on a set of data with homogeneous recording characteristics. The extension of M_m measurements to conventional (i.e., WWSSN) or historical seismograms is currently under way and will be the subject of a separate paper.

5. DISCUSSION OF RESULTS

In order to assess the success of the method, we conduct in this section a critical study of the fit between measured values of the mantle magnitude and published values of the seismic moment, as resulting from moment tensor inversion or other low-frequency seismological techniques. Figure 8 presents all of our data, either split into individual data sets or treated as a whole.

Slope of $\log_{10} M_0$ Versus M_m

First, and for each of the four data sets involved, we regressed the published values of $\log_{10} M_0$ against the corresponding values of M_m computed from (11). The best fitting slopes are 0.95 for the PAS data set, 1.06 for the PPT records, and 1.03 for the GEOSCOPE data set. If all 256 records are regressed together, the best slope is 1.04 . These values do not depart significantly from the slope of 1 expected theoretically; this result and the generally large values of the periods at which the maximum value of M_m is obtained serve as an a posteriori verification of the fact that we indeed stay on the flat portion of the spectrum.

We also attempted to regress $\log_{10} M_0$ versus $[M_m - \log_{10} T]$, where T is the period at which the measurement is made; for all four data sets, this resulted in a deterioration of the quality of the fit, as measured by the root-mean-square residual of the regression, ranging from 25% to 53%. We conclude that our method of measuring M_m does indeed produce a magnitude scale growing linearly with $\log_{10} M_0$ and successfully avoiding the range of saturation effects.

Accuracy of M_m

There remains to discuss the accuracy of the seismic moment values inferred from a single measurement of

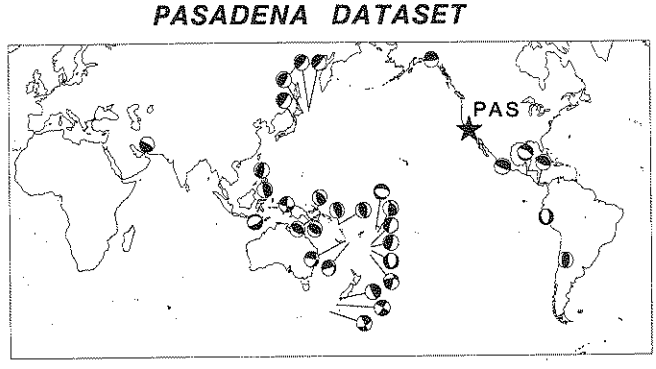

Fig. 6. Map of the epicenters and focal mechanisms for the Pasadena data set.

TABLE 3. Pasadena Data Set

Event	Station	Passage	Δ	M_m^{pub}	M_m	T	r	M_c	r_c
1970 05 31	PAS	1	57.11	8.00	7.76	107.8	-0.24	7.88	-0.12
1970 05 31	PAS	2	302.89	8.00	8.19	85.3	0.19	8.36	0.36
1973 06 17	PAS	1	71.49	7.83	7.47	85.3	-0.36	7.70	-0.13
1975 07 20 A	PAS	1	91.02	7.53	7.55	128.0	0.02	7.12	-0.41
1975 07 20 B	PAS	1	91.22	7.08	7.11	128.0	0.03	6.84	-0.24
1976 08 16	PAS	1	108.86	8.28	8.32	81.9	0.04	8.22	-0.06
1976 08 16	PAS	2	251.14	8.28	8.18	204.8	-0.10	7.96	-0.32
1976 08 16	PAS	3	468.86	8.28	8.36	227.6	0.08	8.13	-0.15
1977 03 18	PAS	1	103.27	6.95	7.02	128.0	0.07	7.16	0.21
1977 04 02	PAS	1	72.12	7.01	7.23	60.2	0.22	7.71	0.70
1977 06 22	PAS	1	79.01	8.15	8.02	107.8	-0.13	8.06	-0.09
1977 06 22	PAS	2	280.99	8.15	7.96	146.3	-0.19	8.13	-0.02
1977 08 19	PAS	1	123.68	8.56	8.14	136.5	-0.42	8.51	-0.05
1977 08 19	PAS	2	236.32	8.56	8.32	240.9	-0.24	8.53	-0.03
1977 08 19	PAS	3	483.68	8.56	8.03	170.7	-0.53	8.34	-0.22
1977 08 19	PAS	4	596.32	8.56	8.08	186.2	-0.48	8.37	-0.19
1977 10 10	PAS	1	80.78	7.01	7.32	128.0	0.31	7.22	0.21
1977 11 23	PAS	1	80.51	7.27	7.61	227.6	0.34	7.35	0.08
1978 03 23	PAS	1	68.92	7.43	7.18	64.0	-0.25	7.56	0.13
1978 03 24	PAS	1	68.94	7.36	7.24	64.0	-0.12	7.55	0.19
1978 06 12	PAS	1	76.43	7.53	7.44	93.1	-0.09	7.75	0.22
1979 02 28	PAS	1	30.53	7.27	7.48	113.8	0.21	7.51	0.24
1979 05 01	PAS	1	87.94	7.16	7.42	107.8	0.26	7.27	0.11
1979 09 12	PAS	1	103.98	7.37	7.95	157.5	0.58	7.59	0.22
1979 09 12	PAS	2	256.02	7.37	7.78	89.0	0.41	7.40	0.03
1979 10 12	PAS	1	105.67	7.00	6.68	170.7	-0.32	6.70	-0.30
1980 07 08	PAS	1	85.22	7.29	7.42	204.8	0.13	7.13	-0.16
1980 07 17	PAS	1	85.67	7.68	7.93	136.5	0.25	7.69	0.01
1980 07 17	PAS	2	274.33	7.68	7.66	128.0	-0.02	7.44	-0.24
1981 05 25	PAS	1	107.57	7.44	7.70	128.0	0.26	7.59	0.15
1981 05 25	PAS	2	252.43	7.44	7.69	85.3	0.25	7.65	0.21
1981 07 06	PAS	1	87.17	7.41	7.30	102.4	-0.11	7.43	0.02
1981 07 28	PAS	1	115.90	6.95	6.99	55.3	0.04	7.07	0.12
1981 09 01	PAS	1	71.57	7.29	7.92	107.8	0.63	7.61	0.32
1981 09 01	PAS	2	288.43	7.29	7.80	107.8	0.51	7.50	0.21
1981 10 25	PAS	1	21.55	6.85	7.11	204.8	0.26	7.21	0.36
1982 06 19	PAS	1	33.39	7.02	7.11	51.2	0.09	7.33	0.31
1982 07 07	PAS	1	110.95	6.83	6.70	73.1	-0.13	7.08	0.25
1982 12 19	PAS	1	79.86	7.30	7.14	53.9	-0.16	7.32	0.02
1983 03 18	PAS	1	91.28	7.67	7.80	78.8	0.13	7.94	0.27
1983 04 03	PAS	1	40.97	7.26	6.82	227.6	-0.44	6.99	-0.27
1986 10 20	PAS	1	82.99	7.95	7.94	227.6	-0.01	8.01	0.06

M_m. For this purpose, we study the population of residuals

$$r = M_m \text{ (measured)} - \log_{10} M_0 \text{ (published)} + 20 \qquad (13)$$

for each of our measurements. Table 6 lists the mean value $\bar{r}$ and standard deviation σ of the residuals for all four data sets. We also list the value for the data set of 20 records measured at PPT in our preliminary study [*Talandier et al.*, 1987]. The significant decrease in the mean value of the residual $\bar{r}$, between the two studies (from 0.18 to 0.02), is due to the use of an improved source correction C_s (see section 3).

We obtained mean residuals $\bar{r}$ in general smaller than 0.2 units. The mean residuals are extremely small at PAS and PPT, somewhat larger at the GEOSCOPE stations. Similarly, the standard deviation σ of the residuals is always less than 0.3 . This means that the measurement of M_m according to (11), once corrected by subtracting $\bar{r}$ at the appropriate station, results in an uncertainty on the value of the seismic moment of a multiplicative or divisive factor f which stays below 2 (we write $f = */10^{\sigma}$). These results must be assessed in the context of the performance of the classical magnitude scales, for which few single stations can boast of having a systematic magnitude bias, and a standard deviation of their magnitude estimates of ~ 0.2 magnitude units. In addition, it is not uncommon for several independent investigators to obtain estimates of M_0 differing by a factor of */ 1.5 to 2.0 .

Investigation of Possible Systematic Biases

In this section we investigate systematically the possible correlation of the residuals r with various parameters, such as distance, period, etc. The existence of any such bias would invalidate one of more assumptions in our theoretical models.

Distance. Figure 9 plots the residuals r as a function

TABLE 4. GEOSCOPE Data Set

Event	Station	Passage	Δ	M_m^{pub}	M_m	T	r	M_c	r_c
1982 06 19	SSB	2	276.61	7.02	7.39	284.4	0.37	7.18	0.16
1982 07 07	SSB	1	162.98	6.83	7.10	160.0	0.27	7.13	0.30
1982 12 19	PCR	1	112.60	7.30	7.36	98.5	0.06	7.55	0.25
1983 01 17	PAF	1	97.81	6.36	6.31	91.4	-0.05	6.98	0.62
1983 01 17	PCR	1	67.84	6.36	6.04	98.5	-0.32	6.52	0.16
1983 01 24	PAF	1	65.51	6.23	6.45	64.0	0.22	6.51	0.28
1983 01 24	PCR	1	50.56	6.23	6.34	256.0	0.11	6.16	-0.07
1983 04 03	PAF	1	133.72	7.26	7.30	256.0	0.04	7.22	-0.04
1983 04 03	PCR	1	138.35	7.26	7.07	232.7	-0.19	7.29	0.03
1983 04 03	SSB	1	82.18	7.26	7.97	256.0	0.71	7.64	0.38
1983 04 04	PAF	1	58.99	6.53	6.79	71.1	0.26	6.70	0.17
1983 04 04	PCR	1	46.92	6.53	6.60	85.3	0.07	6.50	-0.03
1983 04 04	SSB	1	86.16	6.53	6.88	256.0	0.35	6.68	0.15
1983 05 26	PAF	1	108.11	7.66	7.94	256.0	0.28	7.89	0.23
1983 05 26	PCR	2	261.18	7.66	8.09	284.4	0.43	7.78	0.12
1983 05 26	SSB	2	274.63	7.66	7.97	284.4	0.31	7.68	0.02
1983 10 04	PAF	1	96.61	7.53	7.29	256.0	-0.24	7.50	-0.03
1983 10 22	PAF	1	51.10	6.66	7.23	256.0	0.57	6.72	0.06
1983 11 30	PAF	1	42.42	7.61	8.13	213.3	0.52	7.65	0.04
1983 11 30	TAM	1	71.49	7.61	7.82	213.3	0.21	7.86	0.25
1984 01 08	PCR	1	64.06	6.08	6.44	67.4	0.36	6.35	0.27
1984 01 08	TAM	1	112.52	6.08	6.41	256.0	0.33	6.18	0.10
1984 02 07	PCR	1	100.02	7.40	7.79	256.0	0.39	7.46	0.06
1984 02 07	SSB	1	139.10	7.40	7.43	64.0	0.03	7.51	0.11
1984 02 07	PCR	2	259.98	7.40	7.76	284.4	0.36	7.43	0.03
1984 03 24	PCR	1	106.41	6.81	6.83	256.0	0.02	6.89	0.08
1984 03 24	SSB	1	85.14	6.81	7.08	256.0	0.27	6.94	0.13
1984 03 24	TAM	1	105.02	6.81	7.12	256.0	0.31	6.94	0.13
1984 05 17	PCR	1	15.34	6.40	6.18	256.0	-0.22	6.47	0.07
1984 05 17	TAM	1	74.47	6.40	6.80	106.7	0.40	6.43	0.03
1984 05 17	WFM	1	140.03	6.40	6.68	256.0	0.28	6.51	0.11
1984 08 06	TAM	1	104.77	6.46	6.68	65.6	0.22	6.58	0.12
1984 09 18	PCR	1	98.34	6.32	6.55	67.4	0.23	6.43	0.11
1984 09 18	WFM	1	96.82	6.32	6.62	256.0	0.30	6.38	0.06
1984 11 01	PCR	1	96.94	6.60	6.81	128.0	0.21	6.69	0.09
1984 11 01	TAM	1	44.90	6.60	7.04	116.4	0.44	6.70	0.10
1984 11 01	WFM	1	46.54	6.60	7.03	256.0	0.43	6.68	0.08
1984 11 17	PCR	1	46.61	6.76	6.71	256.0	-0.05	6.72	-0.04
1984 11 17	WFM	1	136.77	6.76	6.48	65.6	-0.28	6.62	-0.14
1984 11 23	PCR	1	107.65	6.28	6.58	67.4	0.30	6.50	0.22
1984 11 23	SSB	1	147.10	6.28	6.62	213.3	0.34	6.31	0.03
1984 12 30	PAF	1	72.76	6.26	6.63	116.4	0.37	6.45	0.19
1984 12 30	PCR	1	100.40	6.26	6.57	256.0	0.31	6.43	0.17
1984 12 30	WFM	1	125.88	6.26	6.43	256.0	0.17	6.36	0.10
1985 01 21	PCR	1	73.75	6.15	6.79	67.4	0.64	6.52	0.37
1985 01 21	SSB	1	113.99	6.15	6.72	116.4	0.57	6.46	0.31
1985 01 21	WFM	1	133.64	6.15	6.59	75.3	0.44	7.18	1.03
1985 03 02	PAF	1	63.27	6.04	6.50	80.0	0.46	6.76	0.72
1985 03 02	SSB	1	108.91	6.04	6.71	67.4	0.67	6.97	0.93
1985 03 03	PAF	1	91.08	8.01	7.95	256.0	-0.06	8.08	0.07
1985 03 03	PCR	1	106.25	8.01	8.21	256.0	0.20	8.07	0.06
1985 03 03	SSB	1	104.42	8.01	8.05	256.0	0.04	7.94	-0.07
1985 03 03	TAM	1	92.49	8.01	8.24	256.0	0.23	8.00	-0.01
1985 03 03	WFM	1	75.61	8.01	7.71	256.0	-0.30	8.01	0.00
1985 03 03	PAF	2	268.92	8.01	8.05	213.3	0.04	8.25	0.24
1985 03 03	PCR	2	253.75	8.01	8.18	256.0	0.17	8.04	0.03
1985 03 03	SSB	2	255.58	8.01	8.00	256.0	-0.01	7.90	-0.11
1985 03 03	WFM	2	284.39	8.01	7.78	256.0	-0.23	8.08	0.07
1985 04 09	TAM	1	92.60	6.70	6.91	256.0	0.21	6.73	0.03
1985 04 13	TAM	1	117.67	6.45	6.95	232.7	0.50	6.60	0.15
1985 04 13	WFM	1	131.92	6.45	6.39	85.3	-0.06	6.77	0.32
1985 05 10	PCR	1	93.10	6.84	7.20	128.0	0.36	7.08	0.24
1985 05 10	WFM	1	125.39	6.84	7.21	98.5	0.37	7.11	0.27
1985 07 03	PCR	1	95.12	6.92	7.48	182.9	0.56	7.09	0.17
1985 07 03	AGD	2	249.54	6.92	7.25	94.8	0.33	7.10	0.18
1985 08 23	AGD	1	40.01	6.52	6.60	128.0	0.08	6.85	0.33
1985 08 23	CAY	1	114.56	6.52	6.72	64.0	0.20	6.93	0.41
1985 08 23	PCR	1	63.20	6.52	6.91	182.9	0.39	6.69	0.17
1985 08 23	TAM	1	60.54	6.52	6.73	64.0	0.21	6.87	0.35
1985 09 19	CAY	1	50.79	8.04	7.89	64.0	-0.15	8.64	0.60

TABLE 4. (continued)

Event	Station	Passage	Δ	M_m^{pub}	M_m	T	r	M_c	r_c
1985 09 19	PCR	1	159.22	8.04	7.88	71.1	-0.16	8.64	0.60
1985 09 19	SSB	1	88.64	8.04	8.24	182.9	0.20	8.06	0.02
1985 09 19	CAY	2	309.21	8.04	7.77	256.0	-0.27	8.04	0.00
1985 09 19	SSB	2	271.36	8.04	8.27	256.0	0.23	8.05	0.01
1985 09 21	AGD	1	134.34	7.40	7.68	128.0	0.28	7.55	0.15
1985 09 21	CAY	1	49.89	7.40	7.38	64.0	-0.02	7.70	0.30
1985 09 21	PCR	1	158.31	7.40	7.41	71.1	0.01	7.81	0.41
1985 09 21	SSB	1	88.32	7.40	7.66	182.9	0.26	7.47	0.07
1985 09 21	AGD	2	225.66	7.40	7.65	256.0	0.25	7.47	0.07
1985 09 21	PCR	2	201.69	7.40	7.23	256.0	-0.17	7.47	0.07
1985 09 26	CAY	1	122.37	6.38	6.63	64.0	0.25	6.76	0.38
1985 09 26	PCR	1	104.14	6.38	6.68	116.4	0.30	6.67	0.29
1985 11 17	PCR	1	79.57	6.69	6.99	64.0	0.30	6.75	0.06
1985 11 17	TAM	1	126.66	6.69	7.21	75.3	0.52	6.96	0.27
1985 12 21	AGD	1	125.14	6.76	7.24	256.0	0.48	6.88	0.12
1985 12 21	CAY	1	140.70	6.76	7.24	256.0	0.48	6.90	0.14
1985 12 21	NOC	1	8.11	6.76	6.74	213.3	-0.02	6.93	0.17
1985 12 21	PCR	1	103.66	6.76	7.22	256.0	0.46	6.84	0.08
1985 12 21	WFM	1	120.68	6.76	7.12	256.0	0.36	6.80	0.04
1985 12 23	CAY	1	77.29	6.18	6.76	64.0	0.58	6.36	0.18
1985 12 23	NOC	1	100.40	6.18	6.76	256.0	0.58	6.27	0.09
1985 12 23	SSB	1	65.13	6.18	6.91	75.3	0.73	6.62	0.44
1985 12 23	TAM	1	86.25	6.18	6.88	71.1	0.70	6.53	0.35
1985 12 23	WFM	1	34.94	6.18	6.80	71.1	0.62	6.38	0.20
1986 03 24	AGD	1	96.26	6.05	6.18	64.0	0.13	6.34	0.29
1986 03 24	DRV	1	64.13	6.05	6.10	67.4	0.05	6.45	0.40
1986 03 24	NOC	1	33.18	6.05	6.37	85.3	0.32	6.18	0.13
1986 03 24	SSB	1	121.43	6.05	6.46	64.0	0.41	6.24	0.19
1986 04 20	DRV	1	64.22	6.20	6.30	213.3	0.10	6.33	0.13
1986 04 20	KIP	1	65.65	6.20	6.22	182.9	0.02	6.21	0.01
1986 04 20	NOC	1	32.77	6.20	6.32	64.0	0.12	6.38	0.18
1986 04 20	WFM	1	129.78	6.20	6.49	213.3	0.29	6.29	0.09
1986 04 30	AGD	1	134.95	6.49	6.81	98.5	0.32	6.69	0.20
1986 04 30	CAY	1	51.21	6.49	6.34	182.9	-0.15	6.66	0.17
1986 04 30	DRV	1	117.40	6.49	6.81	256.0	0.32	6.56	0.07
1986 04 30	KIP	1	51.60	6.49	6.34	256.0	-0.15	6.62	0.13
1986 04 30	NOC	1	97.48	6.49	6.65	213.3	0.16	6.63	0.14
1986 04 30	SSB	1	88.73	6.49	6.81	256.0	0.32	6.59	0.10
1986 04 30	TAM	1	98.99	6.49	6.69	256.0	0.20	6.59	0.10
1986 04 30	WFM	1	34.14	6.49	6.82	256.0	0.33	6.59	0.10
1986 05 07	AGD	1	109.23	8.02	8.38	256.0	0.36	8.09	0.07
1986 05 07	CAY	1	105.52	8.02	7.73	284.4	-0.29	7.93	-0.09
1986 05 07	CRZ	1	149.40	8.02	7.87	256.0	-0.15	8.07	0.05
1986 05 07	DRV	1	122.77	8.02	8.16	256.0	0.14	8.01	-0.01
1986 05 07	KIP	1	32.70	8.02	8.27	213.3	0.25	7.98	-0.04
1986 05 07	NOC	1	75.28	8.02	8.14	256.0	0.12	7.97	-0.05
1986 05 07	PAF	1	139.78	8.02	7.86	160.0	-0.16	8.25	0.23
1986 05 07	SSB	1	83.50	8.02	8.35	256.0	0.33	8.08	0.06
1986 05 07	TAM	1	105.96	8.02	8.33	256.0	0.31	8.05	0.03
1986 05 07	WFM	1	63.59	8.02	7.79	256.0	-0.23	7.97	-0.05
1986 05 07	AGD	2	250.77	8.02	8.34	256.0	0.32	8.05	0.03
1986 05 07	CAY	2	254.48	8.02	7.81	284.4	-0.21	8.01	-0.01
1986 05 07	CRZ	2	210.60	8.02	7.82	256.0	-0.20	8.02	0.00
1986 05 07	DRV	2	237.23	8.02	8.17	256.0	0.15	8.02	0.00
1986 05 07	KIP	2	327.30	8.02	8.41	256.0	0.39	8.10	0.08
1986 05 07	NOC	2	284.72	8.02	8.16	256.0	0.14	8.00	-0.02
1986 05 07	PAF	2	220.22	8.02	7.83	284.4	-0.19	8.05	0.03
1986 05 07	SSB	2	276.50	8.02	8.36	256.0	0.34	8.09	0.07
1986 05 07	TAM	2	254.04	8.02	8.30	284.4	0.28	8.01	-0.01
1986 05 07	WFM	2	296.41	8.02	7.77	196.9	-0.25	8.01	-0.01
1986 05 07	AGD	3	469.23	8.02	8.33	284.4	0.31	8.04	0.02
1986 05 07	CAY	3	465.52	8.02	7.76	284.4	-0.26	7.96	-0.06
1986 05 07	CRZ	3	509.40	8.02	8.00	182.9	-0.02	8.29	0.27
1986 05 07	DRV	3	482.77	8.02	8.26	284.4	0.24	8.10	0.08
1986 05 07	KIP	3	392.70	8.02	8.22	256.0	0.20	7.91	-0.11
1986 05 07	NOC	3	435.28	8.02	8.20	284.4	0.18	8.03	0.01
1986 05 07	PAF	3	499.78	8.02	7.84	160.0	-0.18	8.23	0.21
1986 05 07	SSB	3	443.50	8.02	8.35	213.3	0.33	8.09	0.07
1986 05 07	TAM	3	465.96	8.02	8.32	284.4	0.30	8.03	0.01
1986 05 07	WFM	3	423.59	8.02	7.84	256.0	-0.18	8.03	0.01

TABLE 4. (continued)

Event	Station	Passage	Δ	M_m^{pub}	M_m	T	r	M_c	r_c
1986 05 07	AGD	4	610.77	8.02	8.40	232.7	0.38	8.12	0.10
1986 05 07	CAY	4	614.48	8.02	7.85	256.0	-0.17	8.08	0.06
1986 05 07	CRZ	4	570.60	8.02	7.84	111.3	-0.18	8.28	0.26
1986 05 07	DRV	4	597.23	8.02	8.21	284.4	0.19	8.05	0.03
1986 05 07	KIP	4	687.30	8.02	8.45	284.4	0.43	8.13	0.11
1986 05 07	NOC	4	644.72	8.02	8.20	284.4	0.18	8.02	0.00
1986 05 07	PAF	4	580.22	8.02	7.94	111.3	-0.08	8.47	0.45
1986 05 07	SSB	4	636.50	8.02	8.23	284.4	0.21	7.96	-0.06
1986 05 07	WFM	4	656.41	8.02	7.73	196.9	-0.29	7.98	-0.04
1986 07 09	DRV	1	69.21	6.20	6.24	256.0	0.04	6.20	0.00
1986 07 09	KIP	1	75.69	6.20	6.50	256.0	0.30	6.25	0.05
1986 07 09	RER	1	72.92	6.20	6.50	256.0	0.30	6.26	0.06
1986 07 09	SCZ	1	106.31	6.20	6.29	256.0	0.09	6.21	0.01
1986 07 09	SSB	1	110.48	6.20	6.70	256.0	0.50	6.36	0.16
1986 07 09	TAM	1	117.55	6.20	6.73	256.0	0.53	6.31	0.11
1986 08 14	DRV	1	69.07	7.36	7.14	64.0	-0.22	7.21	-0.15
1986 08 14	KIP	1	75.69	7.36	7.40	256.0	0.04	7.50	0.14
1986 08 14	NOC	1	45.46	7.36	7.41	182.9	0.05	7.39	0.03
1986 08 14	PPT	1	84.63	7.36	7.54	128.0	0.18	7.47	0.11
1986 08 14	RER	1	72.91	7.36	7.38	256.0	0.02	7.51	0.15
1986 08 14	SCZ	1	106.36	7.36	7.20	256.0	-0.16	7.61	0.25
1986 08 14	SSB	1	110.62	7.36	7.36	150.6	0.00	7.46	0.10
1986 08 14	TAM	1	117.66	7.36	7.49	256.0	0.13	7.42	0.06
1986 08 14	KIP	2	284.31	7.36	7.48	256.0	0.12	7.60	0.24
1986 08 14	NOC	2	314.54	7.36	7.40	256.0	0.04	7.36	0.00
1986 08 14	PPT	2	275.37	7.36	7.51	213.3	0.15	7.44	0.08
1986 08 14	RER	2	287.09	7.36	7.35	284.4	-0.01	7.48	0.12
1986 08 14	SSB	2	249.38	7.36	7.25	284.4	-0.11	7.34	-0.02
1986 08 14	TAM	2	242.34	7.36	7.52	75.3	0.16	7.41	0.05
			Additional (R_5) Passages for 1986 Aleutian Event						
1986 05 07	AGD	5	829.23	8.02	8.36	111.3	0.34	8.14	0.12
1986 05 07	CAY	5	825.52	8.02	7.99	111.3	-0.03	8.46	0.44
1986 05 07	CRZ	5	869.40	8.02	8.15	196.9	0.13	8.42	0.40
1986 05 07	DRV	5	842.77	8.02	8.18	284.4	0.16	8.02	0.00
1986 05 07	KIP	5	752.70	8.02	8.01	284.4	-0.01	7.70	-0.32
1986 05 07	NOC	5	795.28	8.02	8.05	256.0	0.03	7.88	-0.14
1986 05 07	PAF	5	859.78	8.02	8.01	182.9	-0.01	8.36	0.34
1986 05 07	SSB	5	803.50	8.02	8.37	196.9	0.35	8.12	0.10
1986 05 07	WFM	5	783.59	8.02	8.16	100.4	0.14	8.56	0.54

of the distance Δ at which the measurement is taken. Any significant trend would indicate that our distance correction C_D is inadequate, probably reflecting inappropriate Q models. It is clear from this figure that no such trend exists; a regression of r against $\log_{10}\Delta$ produced a slope of -0.057 for the whole data set, and the steepest slope found was -0.129 for the PAS data set. We further explored the possibility of any systematic bias of M_m with distance through two experiments: first, the data presented in Figure 10*a* show no systematic difference in the residual population between M_m values for first and multiple passages. Then we studied in detail M_m values measured on 10 stations of the GEOSCOPE network following the Aleutian earthquake of May 7, 1986. We use 48 records, including multiple passages up to R_5. The top frames of Figure 10*b* show no systematic trend with distance of the residuals r up to and including R_4. In the case of fifth passages, the signal-to-noise ratio has deteriorated to the point that we may be measuring noise. This explains the trends toward larger and more scattered residuals. In the bottom frames, we compare each residual $r(n)$ for an nth passage to the residual $r(1)$ of R_1 at the same station, thereby eliminating any focal mechanism effect. Again the stability of this new residual with distance is excellent up to and including R_4, but starts to deteriorate for R_5. This justifies a posteriori the elimina-

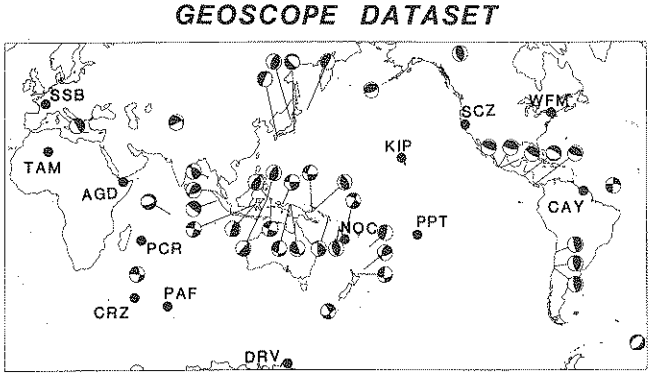

Fig. 7. Map of the epicenters and focal mechanisms for the GEOSCOPE data set. The stations are shown as dots; the post-1986 location of the Réunion Island station (RER), only 18 km away from PCR, is not shown.

TABLE 5. Source Parameters of Events Used in This Study

Date	Epicenter °N	Epicenter °E	Depth, km	Published Moment, 10^{27} dyn-cm	Focal Mechanism ϕ, deg	Focal Mechanism δ, deg	Focal Mechanism λ, deg	Reference
1970 05 31	-9.2	-78.8	33.	10.00	160	37	250	a
1973 06 17	43.0	145.8	33.	6.70	230	27	111	b
1974 10 03	-12.3	-77.7	15.	18.00	160	80	85	c,d
1975 07 20 A	-6.6	155.1	16.	3.40	306	36	90	e
1975 07 20 B	-7.1	155.1	33.	1.20	303	40	90	e
1976 08 16	6.3	124.0	33.	19.00	327	22	68	f
1977 03 18	16.8	122.3	35.	0.89	207	27	108	g
1977 04 02	-16.7	-172.1	50.	1.03	317	41	45	g
1977 04 21	-10.0	160.7	40.	1.20	326	35	79	g
1977 06 22	-22.9	-175.9	61.	14.00	197	79	271	g
1977 08 19	-11.1	118.5	23.	36.00	260	24	287	g
1977 10 10	-25.9	-175.4	23.	1.02	18	38	293	g
1977 11 23	-31.0	-67.8	21.	1.86	183	44	90	g
1978 03 23	44.1	149.0	28.	2.70	224	11	91	h
1978 03 24	144.2	148.9	31.	2.30	223	18	93	h
1978 06 12	38.2	142.0	38.	3.40	184	14	59	h
1978 11 29	16.0	-96.6	16.	5.27	127	84	94	h
1979 02 16	-16.4	-72.7	34.	0.62	59	16	25	i
1979 02 28	60.6	-141.6	19.	1.90	271	13	96	i
1979 03 14	17.8	-101.3	27.	1.72	306	15	110	i
1979 05 01	-21.2	169.8	73.	1.45	18	41	190	i
1979 09 12	-1.7	136.0	16.	2.40	100	71	5	i
1979 10 12	-46.7	165.7	20.	1.00	19	15	136	i
1980 07 08	-12.4	166.4	44.	2.00	157	42	78	j
1980 07 17	-12.6	165.9	34.	4.85	351	31	102	j
1981 05 25	-48.8	164.4	33.	2.75	302	83	355	k
1981 07 06	-22.3	171.7	58.	2.60	345	30	181	k
1981 07 15	-17.3	167.6	30.	0.58	338	27	83	k
1981 07 28	30.0	57.8	15.	0.90	150	13	119	k
1981 09 01	-15.0	-173.1	20.	1.95	115	37	287	k
1981 10 25	18.0	-102.1	32.	0.70	287	20	82	k
1982 06 07 A	16.6	-98.2	11.	0.29	268	10	48	l
1982 06 07 B	16.6	-98.3	19.	0.27	286	12	76	l
1982 06 19	13.3	-89.3	52.	1.05	102	25	254	l
1982 07 07	-51.2	160.5	10.	0.68	65	62	182	l
1982 08 05	-12.7	165.9	24.	0.32	337	32	83	l
1982 12 19	-24.1	-175.9	30.	1.98	198	15	90	l
1983 01 17	38.1	20.2	10.	0.23	34	14	153	m
1983 01 24	12.9	93.6	73.	0.17	291	50	39	m
1983 03 18	-4.9	153.6	70.	4.63	170	49	120	m
1983 04 03	8.7	-83.1	28.	1.82	310	25	110	n
1983 04 04	5.7	94.8	72.	0.34	207	51	51	n
1983 05 26	40.4	139.1	13.	4.60	16	27	86	n
1983 10 04	-26.6	-70.8	39.	3.40	9	20	110	o
1983 10 22	-60.6	-25.4	10.	0.46	231	35	278	o
1983 11 30	-6.9	72.1	10.	4.10	293	35	308	o
1984 01 08	-2.8	118.8	15.	0.12	13	16	85	p
1984 02 07	-9.9	160.5	22.	2.50	296	37	30	p
1984 03 24	44.2	148.3	31.	0.64	229	17	109	p
1984 05 17	-36.5	53.5	10.	0.25	1	64	177	q
1984 08 06	32.4	131.8	29.	0.29	337	7	224	r
1984 09 19	34.0	141.4	35.	0.21	264	26	220	r
1984 11 01	8.1	-38.8	10.	0.40	274	73	183	s
1984 11 17	0.2	98.0	25.	0.58	334	10	116	s
1984 11 23	-14.3	171.3	27.	0.19	300	66	353	s
1984 12 30	-36.7	177.5	19.	0.18	86	56	348	s
1985 01 21	-1.0	128.5	21.	0.14	203	76	188	t
1985 03 02	-2.0	119.7	44.	0.11	283	84	357	t
1985 03 03	-33.2	-72.0	41.	10.30	11	26	110	t
1985 04 09	-34.2	-71.5	47.	0.50	0	21	99	u
1985 04 13	1.7	126.6	40.	0.28	12	34	69	u
1985 05 10	-5.6	151.1	25.	0.69	193	67	194	u
1985 07 03	-4.5	152.8	31.	0.83	169	37	106	v
1985 08 23	39.4	75.3	15.	0.33	315	29	159	v
1985 09 19	18.2	-102.6	21.	11.00	301	18	105	v
1985 09 21	17.8	-101.7	21.	2.50	296	17	85	v
1985 09 26	-34.6	-178.7	61.	0.24	196	54	39	v
1985 11 17	-1.6	135.0	13.	0.49	179	64	174	w

TABLE 5. (continued)

Date	Epicenter °N	Epicenter °E	Depth, km	Published Moment, 10^{27} dyn-cm	Focal Mechanism ϕ, deg	Focal Mechanism δ, deg	Focal Mechanism λ, deg	Reference
1985 11 28 A	-14.0	166.2	24.	0.30	161	36	251	w
1985 11 28 B	-14.0	166.2	44.	0.36	262	68	13	w
1985 12 21	-14.0	166.5	46.	0.57	165	44	85	w
1985 12 23	62.2	-124.3	15.	0.15	354	45	98	w
1986 03 24	-2.5	138.7	15.	0.11	94	39	356	x
1986 04 20	-2.4	139.3	21.	0.16	88	29	20	y
1986 04 30	18.4	-102.9	21.	0.31	290	18	87	y
1986 05 07	51.4	-174.8	23.	10.40	246	22	85	y
1986 07 09	2.0	126.6	35.	0.16	9	39	71	z
1986 08 14	1.8	126.6	20.	2.30	224	81	104	z
1986 10 20	-28.1	-176.4	50.	9.00	270	56	158	aa,ab,ac
1987 02 08	-5.9	147.8	15.	1.11	82	83	4	ad
1987 03 05	-24.5	-70.2	42.	2.48	12	23	106	ad
1987 03 06	0.15	-77.8	15.	0.64	113	24	183	ad
1987 06 27	-2.2	138.2	27.	0.08	118	53	5	ae
1987 07 06	-14.1	167.8	15.	0.10	159	42	84	af
1987 08 08	-19.0	-70.0	79.	0.79	176	20	273	af
1987 09 03	-58.90	158.30	15.	1.40	155	69	188	af
1987 09 28 A	-18.45	168.11	23.	0.19	346	25	98	af
1987 09 28 B	-18.36	168.14	22.	0.08	349	26	105	af

References: a, *Abe* [1972]; b, *Shimazaki* [1974]; c, *Dewey and Spence* [1979]; d, *Kanamori* [1977]; e, *Lay and Kanamori* [1980]; f, *Stewart and Cohn*[1979]; g, *Dziewonski et al.* [1987*a*]; h, *Dziewonski et al.* [1987*b*]; i, *Dziewonski et al.* [1987*c*]; j, *Dziewonski et al.* [1988*a*]; k, *Dziewonski et al.* [1988*b*]; l, *Dziewonski et al.* [1983*a*]; m, *Dziewonski et al.* [1983*b*]; n, *Dziewonski et al.* [1983*c*]; o, *Dziewonski et al.* [1984*a*]; p, *Dziewonski et al.* [1984*b*]; q, *Dziewonski et al.* [1985*a*]; r, *Dziewonski et al.* [1985*b*]; s, *Dziewonski et al.* [1985*c*]; t, *Dziewonski et al.* [1985*d*]; u, *Dziewonski et al.* [1986*a*]; v, *Dziewonski et al.* [1986*b*]; w, *Dziewonski et al.* [1986*c*]; x, *Dziewonski et al.* [1987*d*]; y, *Dziewonski et al.* [1987*e*]; z, *Dziewonski et al.* [1987*f*]; aa, *Dziewonski et al.* [1987*g*]; ab, *Lundgren and Okal* [1988]; ac, B. Romanowicz and T. Monfret (personal communication, 1987); ad, *Dziewonski et al.* [1988*c*]; ae, *Dziewonski et al.* [1988*d*]; af, *Dziewonski et al.* [1988*e*].

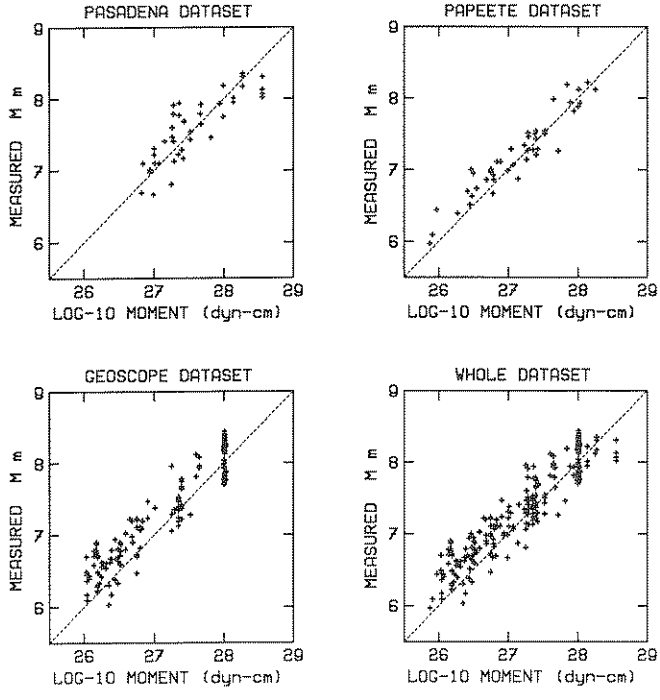

Fig. 8. Full populations of M_m values plotted as a function of published moment M_0, either as individual data sets (top; lower left), or as a whole data set (lower right). In all cases, the dashed line is the expected relation $M_m = \log_{10} M_0 - 20$.

tion of the R_S values from the data sets described in the previous sections. On the basis of these various experiments, we conclude that the corrections C_D are adequate.

In another test we isolated the 10 records with the shortest epicentral distances. The latter vary between 8.11° and 32.77°, with seismic moments ranging from 1.6×10^{26} to 1.4×10^{28} dyn-cm. As Table 6 and Figure 11 show, there is no anomalous trend for these measurements taken at short distances. This means that the accuracy of the M_m scale is still appropriate at distances as short as 8° (Vanuatu event of December 21, 1985 recorded at Nouméa). This result is crucial for tsunami warning. At such short distances, less than an hour separates the passage of the surface wave from the arrival of the tsunami, and there may not be time to wait for surface wave reports from other Pacific stations.

Periods. Figure 12 similarly shows the residuals r as a function of the period T at which the measurement is taken. Since the previous test has suggested that the period-dependent C_D is not systematically biased, any significant trend would indicate that our corrections C_S are inadequate or that we suffer from source finiteness effects. Again, it is clear from Figure 12 that no such trend exists; a regression of r against $\log_{10} T$ produced a slope of -0.021 (or less than 0.01 magnitude unit per octave) for the whole data set, and the maximum value was -0.149 at PAS. Our conclusion is, again, that no significant bias is evidenced by this analysis.

TABLE 6. Averages and Standard Deviations of the Residuals r.

Data Set	Station Code	Number of Records	$\bar{r}$	σ	$\bar{r}_c$	σ_c
Whole data set		256	0.14	0.25	0.09	0.19
Pasadena	PAS	42	0.02	0.28	0.05	0.23
Papeete	PPT	45	0.09	0.19	-0.05	0.16
GEOSCOPE		169	0.18	0.24	0.13	0.17
Special Sub-Data Sets						
PPT subset [*Talandier et al.*, 1987]	PPT	20	0.02	0.18	-0.10	0.13
10 shortest distances		10	0.07	0.15	0.08	0.17
Individual GEOSCOPE *Stations*						
Pointe des Cafres, Réunion†	PCR,RER	31	0.18	0.24	0.14	0.14
Saint-Sauveur de Badole, France	SSB	25	0.31	0.21	0.14	0.21
Tamanrasset, Algeria	TAM	19	0.33	0.15	0.12	0.11
Westford, Massachusetts	WFM	18	0.10	0.31	0.12	0.24
Port-aux-Français, Kerguelen Islands	PAF	16	0.11	0.26	0.22	0.21
Cayenne, French Guyana	CAY	12	0.00	0.29	0.17	0.20
Arga, Djibouti	AGD	11	0.29	0.11	0.14	0.10
Nouméa, New Caledonia	NOC	11	0.17	0.15	0.06	0.08
Dumont d'Urville, Antarctica	DRV	9	0.11	0.14	0.06	0.14
Kipapa, Hawaii	KIP	9	0.18	0.18	0.07	0.10
Crozet Island††	CRZ	4	-0.14	0.07	0.14	0.12
Santa Cruz, California††	SCZ	2	-0.04	0.13	0.13	0.12
Papeete, Tahiti††	PPT	2	0.16	0.02	0.10	0.02
Time Domain Measurements						
Papeete	PPT	45	-0.07	0.22	-0.16	0.17

†We treat as a single dataset records from the Réunion Island station before and after it was moved (about 18 km) to Rivière de l'Est (RER) in 1986.

††Due to the small number of events, the values obtained at these stations may not be statistically significant.

We found little systematic correlation between the period yielding the largest M_m and M_m itself. In general, the biggest earthquakes in our data set have M_m measured at periods over 100 s. A notable exception is the Kermadec earthquake (October 20, 1986). Significantly, this is an event for which available estimates of M_0 vary widely. The Harvard CMT solution for this event ($M_0 = 4.52 \times 10^{27}$ dyn-cm) is significantly less than

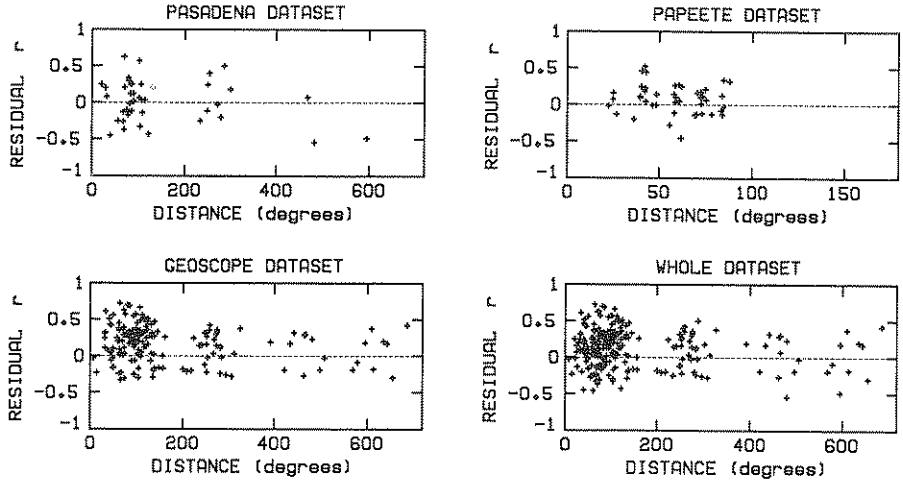

Fig. 9. Residual population $r = M_m - \log_{10} M_0 + 20$ plotted as a function of distance Δ. The horizontal scale is different at PPT, where we have no multiple passages. Any systematic trend on these diagrams would invalidate the correction C_D and probably the Q models.

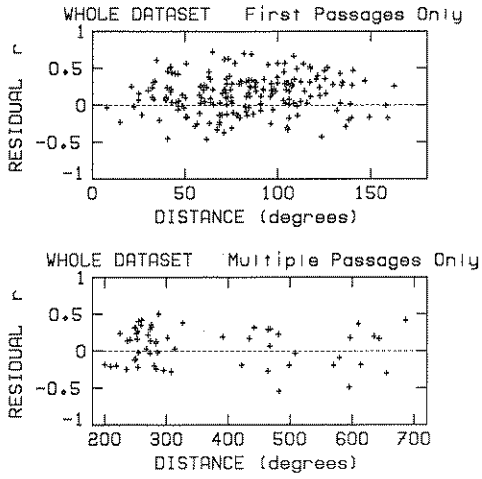

Fig. 10*a*. Comparison of residual populations plotted as a function of distance for first and multiple passages, respectively. Any systematic difference between trends on these diagrams would indicate an inappropriate C_D.

reported by other investigators: *Lundgren and Okal* [1989] have proposed $(8.5–10) \times 10^{27}$ on the basis of body wave deconvolution and B. Romanowicz and T. Monfret (personal communication, 1987) have obtained 9×10^{27} from the GEOSCOPE data set. We obtain values of M_m of 7.83 at PPT and 7.94 at PAS, in much better agreement with the higher values. It is noteworthy that the PPT measurement is obtained at a period of only 63 s, a clear anomaly for an earthquake this size. Similarly, while M_m at PAS is obtained at a longer period (227 s), the value measured at 51 s is very large (7.85). *Lundgren and Okal* [1988] have shown that this event is characterized by a body wave source spectrum anomalously rich in high frequencies. This earthquake is an example of how the use of M_m can retrieve valuable information on the source characteristics of the earthquake in the form of the period T at which the final measurement is made.

Influence of focal mechanism and depth. The most far-reaching approximation that we made in deriving the expression of M_m is the replacement of the true excitation E by its average taken over many focal geometries and depths. In this section we investigate systematically the influence of the source characteristics on our measurements. In keeping with the concept of magnitude, we do not envision incorporating a correction for focal geometry into the computation of M_m; the purpose of this section is simply to assess whether the residuals r are due significantly to the effects of radiation pattern and depth.

Focal mechanism and depth information is listed in Table 5 for all earthquakes used in this study. For each record we use (8) to compute the true excitation E in the exact focal and receiver geometry. We then define the "focal mechanism contribution" as

$$C_{FM} = -\log_{10} E - C_S \tag{14}$$

and a corrected value of M_m as

$$M_c = M_m + C_{FM} \tag{15}$$

M_c is the value of M_m which we would have computed at the same period had we known the focal mechanism exactly, instead of using the average excitation (10). Values of M_c and of the residual $r_c = M_c - \log_{10} M_0 + 20$, are listed as the last two columns of Tables 2–4. We then conducted some statistical analyses on r_c similar to those in section 4. Results are shown in the last two columns of Table 6.

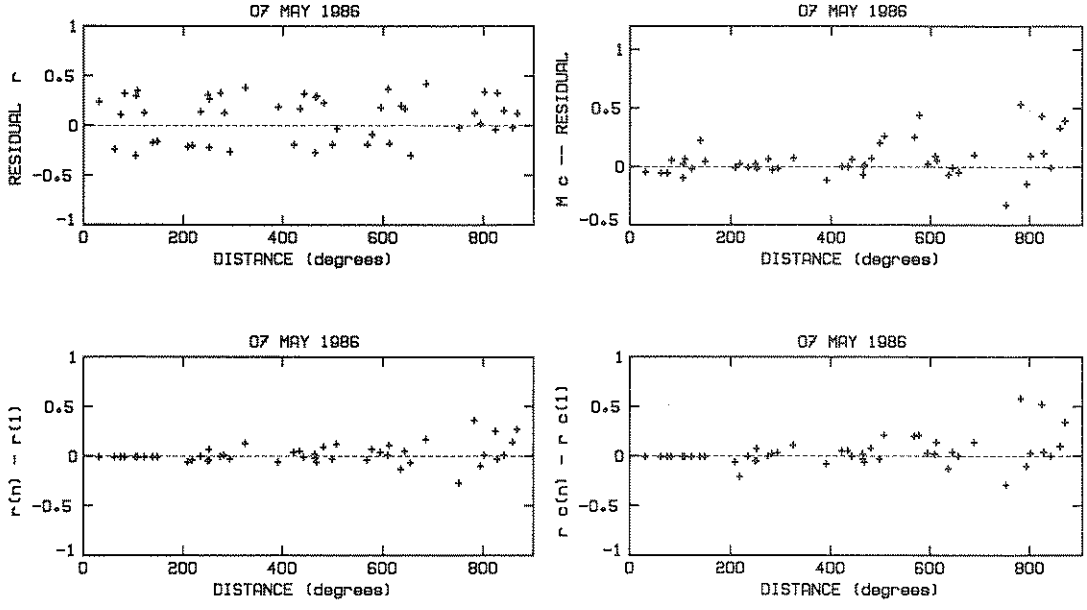

Fig. 10*b*. Residual population for 48 GEOSCOPE records of the 1986 Aleutian event, up to and including R_5. (Top Left) Same as Figure 9. (Bottom Left) The residual $r(n)$ for each passage R_n has been subtracted from the fundamental $r(1)$ at the same station. (Right) Same as left, for the corrected values r_c (see text and Figure 13 for details).

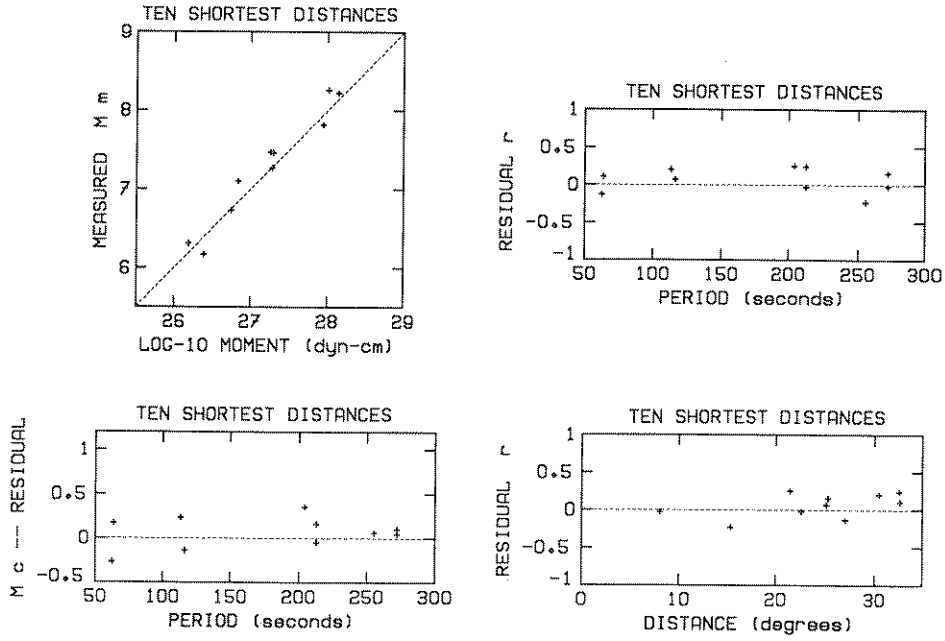

Fig. 11. Same as Figures 8, 9, 12, and 13 for the 10 shortest paths. Note the absence of any systematic trend which could invalidate the use of M_m at regional distances.

The average absolute value of C_{FM} is 0.21 or 0.22 for all four data sets. Not surprisingly, the mean residuals $\bar{r}_c$ and standard deviations σ_c computed for the M_c data sets are generally improved with respect to their M_m counterparts. The only exception is $\bar{r}_c$ at PAS, but the difference (0.03 units of magnitude) is not significant. The variance reduction introduced by the use of C_{FM} is rather limited, on the order of only 30–40%. In some individual cases the inclusion of C_{FM} results in a significant deterioration of the estimate of M_0. Examples are the Samoa event (April 2, 1977) at PAS and the Mexican earthquake (September 19, 1985) at Cayenne. These are cases when the station is located close to a node of excitation of the published mechanism, and yet significant energy is found in the seismogram. There may be two reasons for this situation: either inaccuracy in the published focal mechanism (and/or depth) or multipathing due to lateral heterogeneity, resulting in a distorted value of the take-off azimuth ϕ_s in (8). The latter is suggested by the observation that the large r_c residuals occur preferentially at shorter periods, as shown on Figure 13. In such geometries it actually makes sense to use the concept of magnitude which is found to be more robust than a measurement taking into account a supposedly exact value of

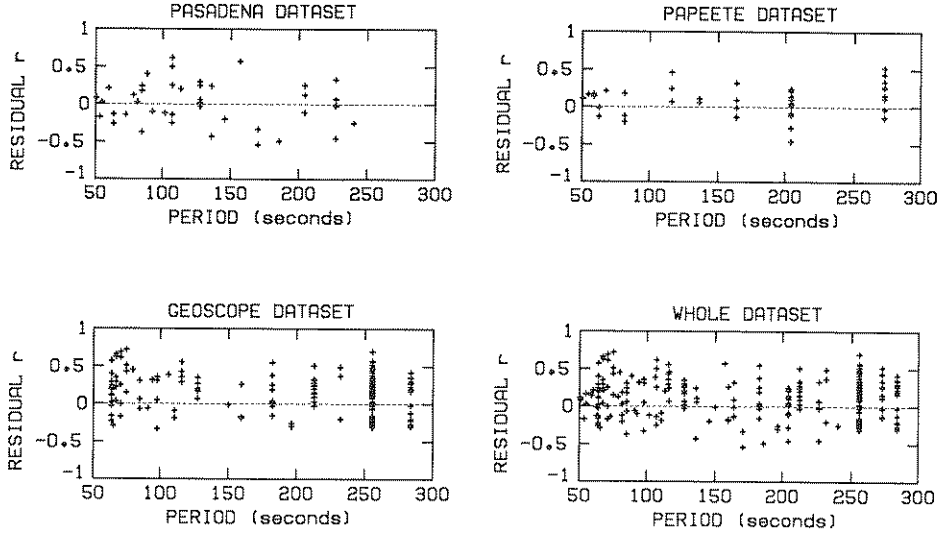

Fig. 12. Residual population $r = M_m - \log_{10} M_0 + 20$ plotted as a function of the period T at which the measurement is taken. Any systematic trend on these diagrams would invalidate C_S or the assumption that we stay on the flat portion of the spectrum.

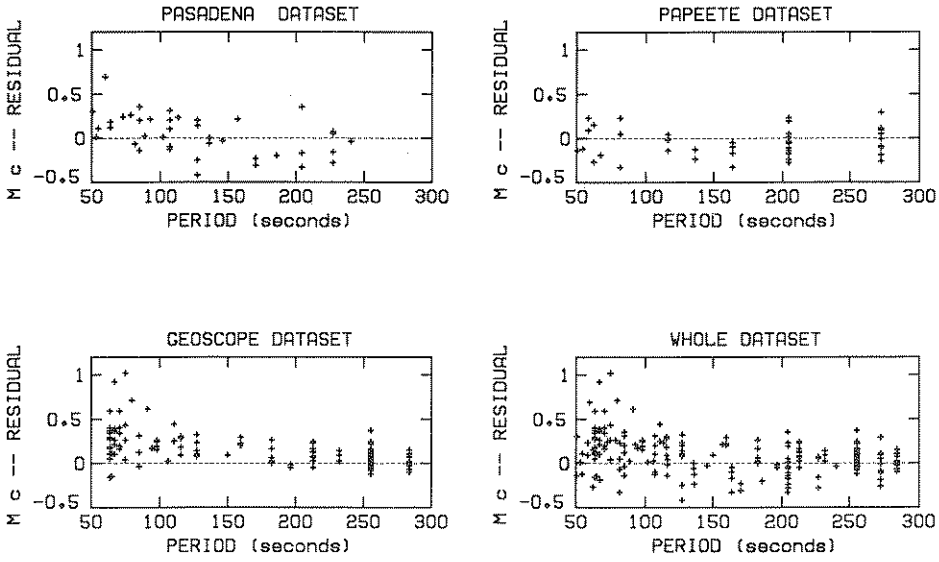

Fig. 13. Same as Figure 12 for the corrected residuals $r_c = r + C_{FM}$. Note that the largest residuals occur at the short-period end of the spectrum, suggesting that multipathing may be responsible.

the excitation, which can be strongly affected by phenomena such as multipathing or incorrect values of the source parameters.

Finally, Table 3 shows that the somewhat deficient values of M_m for the largest earthquake in the data set (the 1977 Indonesian event) are an artifact of the use of a single station (PAS) at an unfavorable azimuth, rather than the expression of saturation.

Station corrections? We also investigated any possible systematic trends in r at individual stations. We are motivated in this respect by the common practice of using "station corrections" for magnitude scales measured at higher frequencies, although we would expect them to disappear at longer periods. Table 6 shows the values of $\bar{r}$ and σ at individual stations. Most values of $\bar{r}$ fall within the 0.1—0.2 range, with the exception of the GEOSCOPE stations AGD (Djibouti), TAM (Tamanrasset, Algeria), and SSB (Saint-Sauveur, France), which have values of $\bar{r}$ in the 0.29–0.33 range. The general proximity of these three stations could suggest some kind of lateral heterogeneity effect. However, this pattern disappears when the M_c values are used, indicating that the higher residuals at these three stations are an artifact of preferential focal geometry. We do not have a simple explanation for the fact that the GEOSCOPE data set has $\bar{r}_c$ slightly larger than PAS (by 0.08 units) and PPT (by 0.13 units). Also, the results are probably not significant at SCZ (Santa Cruz, California) and PPT (GEOSCOPE station, Papeete) for each of which we have only two records and at CRZ (Crozet Island), for which all four records pertain to the Aleutian event of May 7, 1986.

We currently do not have a satisfactory explanation of the global residual $\bar{r} = 0.14$. We have shown in the previous sections that r has no systematic correlation with distance, period, or station. In general, by using an average excitation instead of the exact focal mechanism, we introduce a slight bias amounting to 0.05 units of magnitude. The remaining $\bar{r}_c = 0.09$ must be considered an unexplained bias inherent in the methodology. The small amplitude of this number constitutes in itself one of the successes of the theory. Only the future application of this method to much larger data sets could conceivably help answer this question.

Path. Finally, we want to discuss the possible influence on the computed value of M_m of the tectonic nature of the particular path involved. The calculation of C_D in (6) uses regionalized values of the group velocity U and attenuation factor Q^{-1}: this practice is motivated by the difficulty of defining a single value of these parameters (especially attenuation) at each frequency. However, the question then arises of the stability of M_m measurements with respect to a change in tectonic model or, in practical terms, how erroneous will be our estimate of the seismic moment M_0 if we happen to use the wrong tectonic model for U and Q.

We examined this question in several ways. First, we considered pure paths, assumed to sample only provinces of homogeneous tectonic character. For periods ranging from 50 to 300 s and for distances varying between 5 and 115°, we computed all seven values of C_D and retained their range of variation. This quantity, directly expressed in units of magnitude, is contoured on Figure 14. As expected, the range of variation of C_D is important only for short periods and large distances. It remains below 0.1 unit of magnitude over most of the distance-period field. In addition, these calculations are clearly made under a worst case scenario: for example, the maximum range of variation of nearly 1.0 unit of magnitude would correspond to the case of a 50-s wave traveling 115° in a pure shield structure and mistakenly interpreted as traveling the same distance over a "trench and back arc" region. Either path is geographically impossible at the surface of the Earth; in the real world the lateral heterogeneity of the planet acts to reduce considerably the range of variations of C_D over realistic paths.

In turn, this observation led us to assess the validity of

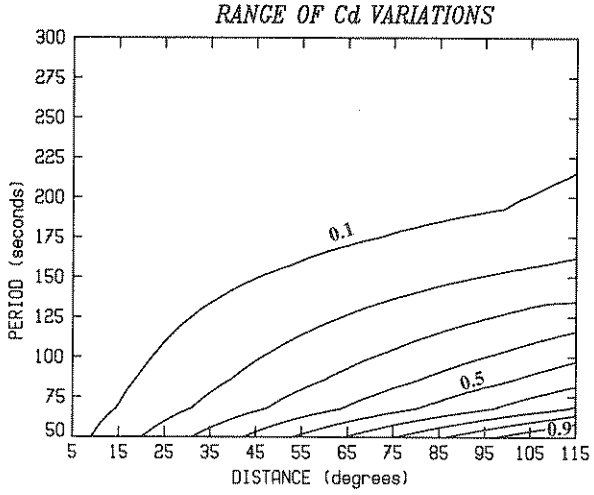

Fig. 14. Range of variation of C_D with tectonic province, as a function of distance and period. Contoured (in units of magnitude) is the difference between the maximum and minimum values of C_D obtained by applying (6) to seven pure paths sampling exclusively the seven tectonic regions described in Table 1.

using an average model of U and Q in the computation of C_D. Specifically, at each period we define

$$U_{aver} = \frac{1}{7} \sum_{k=1}^{7} U_k \tag{16}$$

and

$$Q_{aver}^{-1} = \frac{1}{7} \sum_{k=1}^{7} Q_k^{-1} \tag{17}$$

where the index k is related to tectonic region (note that as a further simplifying assumption, these averages are not weighted in proportion to the true extent of each region at the surface of the Earth). We then used the PPT data set to compare the resulting corrections C_D^{aver} to the actual corrections obtained through regionalization and used in the compilation of Table 2. The average error thus introduced was found to be less than 0.01 unit of magnitude, and its root mean square is 0.03 units of magnitude. The largest value, obtained for the 1986 Kermadec earthquake, is 0.06 units. A similar experiment on first passages R_1 at PAS yields an average of 0.01 unit of magnitude, a root mean square error of 0.03 units, and a maximum value of 0.06 unit for the 1977 Samoa event. In view of the general precision of our method, we believe that these errors are negligible.

The argument could then be made that regionalization may be superfluous and that the use of C_D^{aver} is satisfactory. For spectral measurements taken in the frequency domain, and thus requiring computer processing, regionalization is straightforward and can be achieved at very little programming cost. As we discuss below, our method can be extended to the time domain and applied in the absence of computer support. Our results show that in this latter case, the use of an average tectonic model should not lead to significant errors. With such an application in mind, and for reference, we compile in Table 7 values of C_D^{aver} at a number of representative distances and periods. We also include the distance-independent source correction C_S; their combination allows immediate use of (11) or (19) (for the latter, see the time-domain discussion below).

6. Extension to Time-Domain Measurements

All of the previous theory and measurements were taken in the frequency domain. However, the notion of magnitude was developed primarily in the time domain, and it may be interesting to extend the concept of M_m to time domain measurements.

It is tempting, on a seismogram such as shown on Figure 1, to measure the amplitudes of the prominent oscillations of the Rayleigh wavetrain in its inversely dispersed period range (typically between 50 and 250 s) and to use them to characterize the earthquake's size. In this section we present a simple, phenomenological, justification of this concept. A more rigorous investigation of the relationship of time domain magnitudes and seismic moment, based on phase-stationary asymptotics to the Fourier integral, is given in a companion paper [*Okal*, this issue].

At short distances the inversely dispersed portion of the Rayleigh wave often can be modeled as a single full oscillation of a sinusoid of period T_0 (see Figure 15). The Fourier amplitude of such a signal at the corresponding angular frequency $\omega_0 = 2\pi/T_0$ is related to the zero-to-peak amplitude a_0 of the apparent sinusoid through

$$X(\omega_0) = \frac{1}{2} a_0 T_0 \tag{18}$$

Away from ω_0, the spectral amplitude falls off as the function sinc $[\frac{1}{2} (\omega - \omega_0) T_0]$.

As the distance becomes larger, the waveform becomes more dispersed, and several oscillations with clearly increasing periods are identifiable (Figure 1). We make the simplifying assumption that each oscillation is sufficiently different in frequency from the previous one, so that when computing the spectral amplitude at its

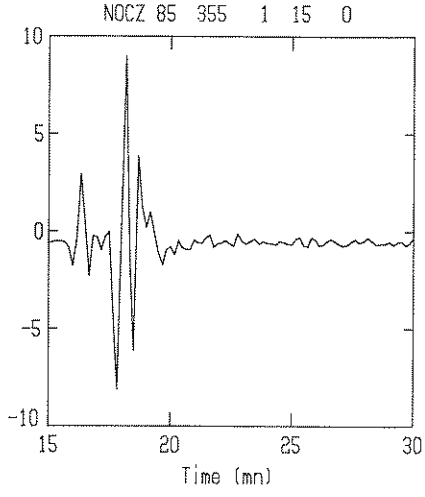

Fig. 15. Example of a Rayleigh wave at very short distances (Vanuatu event of December 21, 1985 at Nouméa), clearly showing one prominent oscillation at a period $T \sim 45$ s.

TABLE 7. Source Correction C_S According to (10), and Distance Correction C_D^{aver} for an Average Earth Model, as a Function of Period and Distance

Distance, deg	Corrections (Magnitude Units) at Various Periods T										
	T = 50 s	T = 75 s	T = 100 s	T = 125 s	T = 150 s	T = 175 s	T = 200 s	T = 225 s	T = 250 s	T = 275 s	T = 300 s
	Correction C_S (Independent of Distance)										
	3.674	3.746	3.781	3.805	3.826	3.847	3.870	3.895	3.922	3.951	3.982
	Correction C_D^{aver}										
5	-0.498	-0.506	-0.511	-0.515	-0.518	-0.520	-0.521	-0.522	-0.523	-0.524	-0.525
10	-0.317	-0.332	-0.343	-0.350	-0.355	-0.360	-0.363	-0.365	-0.367	-0.369	-0.370
15	-0.198	-0.221	-0.237	-0.249	-0.256	-0.263	-0.268	-0.271	-0.274	-0.277	-0.279
20	-0.106	-0.137	-0.158	-0.173	-0.184	-0.192	-0.199	-0.203	-0.207	-0.211	-0.213
25	-0.028	-0.067	-0.093	-0.112	-0.125	-0.136	-0.144	-0.150	-0.155	-0.159	-0.163
30	0.040	-0.006	-0.038	-0.061	-0.077	-0.090	-0.099	-0.106	-0.112	-0.117	-0.121
35	0.101	0.048	0.011	-0.016	-0.034	-0.050	-0.061	-0.069	-0.076	-0.082	-0.087
40	0.158	0.096	0.054	0.024	0.003	-0.015	-0.027	-0.037	-0.045	-0.051	-0.057
45	0.210	0.141	0.094	0.059	0.036	0.016	0.002	-0.009	-0.018	-0.025	-0.031
50	0.259	0.182	0.130	0.092	0.066	0.044	0.028	0.016	0.006	-0.002	-0.009
55	0.306	0.221	0.163	0.121	0.092	0.069	0.051	0.038	0.027	0.018	0.010
60	0.349	0.257	0.194	0.148	0.117	0.091	0.072	0.057	0.046	0.036	0.027
65	0.391	0.291	0.223	0.173	0.139	0.111	0.090	0.075	0.062	0.051	0.042
70	0.431	0.323	0.250	0.196	0.159	0.129	0.106	0.090	0.076	0.065	0.055
75	0.468	0.353	0.274	0.217	0.178	0.145	0.121	0.103	0.089	0.076	0.066
80	0.504	0.381	0.297	0.236	0.194	0.159	0.134	0.115	0.099	0.086	0.075
85	0.538	0.408	0.319	0.254	0.209	0.172	0.145	0.125	0.108	0.094	0.082
90	0.571	0.433	0.338	0.269	0.222	0.183	0.154	0.133	0.116	0.101	0.088
95	0.602	0.456	0.356	0.283	0.234	0.192	0.162	0.139	0.121	0.106	0.092
100	0.631	0.477	0.372	0.296	0.243	0.200	0.168	0.144	0.125	0.109	0.094
105	0.659	0.497	0.387	0.307	0.252	0.206	0.172	0.147	0.127	0.110	0.095
110	0.684	0.515	0.400	0.316	0.258	0.210	0.175	0.149	0.128	0.110	0.094
115	0.708	0.531	0.411	0.323	0.262	0.212	0.176	0.148	0.126	0.107	0.091

exact frequency, we can neglect the side lobes of the other sinc functions. *Okal and Talandier* [1987] tested this assumption on a very crude model of the Rayleigh waveform and found that it should not introduce an error of more than ±0.15 orders of magnitude. Under these conditions we can substitute (18) into (11) and obtain the time domain mantle magnitude

$$M_m^{TD} = \log_{10} [a\ T] + C_S + C_D - 1.20 \qquad (19)$$

where a is the zero-to-peak amplitude in microns, T the period in seconds of a prominent oscillation of the long-period inversely dispersed Rayleigh wave, and C_D and C_S are given by (6) and (10).

Comparison With Data

In order to test the concept of a time-domain mantle magnitude, we computed M_m^{TD} values from (19) for 42 records at Papeete. As in the case of spectral measurements, we take measurements at all prominent periods, and retain the largest value of M_m^{TD}. In order to stay in the well-dispersed part of the spectrum, and as suggested from *Okal* [this issue], we restrict ourselves to the period range 60–200 s. Results are given in Table 8 and Figure 16. The average residual $\bar{r}^{TD}$ for the entire data set of 42 events is -0.07, and the standard deviation $\sigma^{TD} = 0.22$. As in the case of spectral amplitudes, we computed the influence of the exact focal mechanism and depth of the event on the residual; again, we find a slight improvement of σ^{TD} but in this case a deterioration of the mean residual. These values are compiled as part of Table 6. The populations of residuals obtained in the time and frequency domains are comparable in mean values and standard deviations. However, direct comparison between individual values for the same event is not significant, since the two measurements can be taken at different periods.

Other Extensions of M_m: a Perspective

It would be simple in principle to extend the concept of M_m in at least two other directions.

An extension to Love waves could provide an additional safeguard against the problem of a nodal station, since it is well known that for "pure" mechanisms Rayleigh nodes are Love maxima, and vice-versa. M_m can then be defined as the greater of $M_m^{Rayleigh}$ and M_m^{Love}. The computation of the source correction C_S is straightforward. The distance correction requires the compilation of new models of Q and U. Because Love waves are not efficiently dispersed, prominent frequencies are difficult to identify in their wave shapes, and thus we do not expect that a time domain M_m^{Love} could be defined.

It is also possible to extend the M_m concept to deeper earthquakes. While the motivation of accurate tsunami warning no longer exists, it is still useful to develop a simple one-station mantle magnitude for such events. The

TABLE 8. Time Domain Measurements at Papeete

Event	Station	Passage	Δ	M_m^{pub}	M_m^{TD}	T	r^{TD}	M_c^{TD}	r_c^{TD}
1973 06 17	PPT	1	84.68	7.85	7.77	148	-0.08	7.51	-0.34
1974 10 03	PPT	1	69.18	8.26	7.99	149	-0.27	7.94	-0.32
1977 04 02	PPT	1	21.54	7.03	6.97	69	-0.06	6.92	-0.11
1977 06 22	PPT	1	25.24	8.15	8.01	88	-0.14	7.70	-0.45
1978 03 24	PPT	1	83.32	7.36	7.06	158	-0.30	7.03	-0.33
1978 06 12	PPT	1	84.80	7.53	7.03	171	-0.50	6.99	-0.54
1979 02 16	PPT	1	73.03	6.79	6.42	141	-0.37	6.69	-0.10
1979 02 28	PPT	1	78.34	7.27	7.01	140	-0.26	6.91	-0.36
1979 03 14	PPT	1	59.17	7.24	7.10	158	-0.14	7.07	-0.17
1979 10 12	PPT	1	46.82	7.00	6.73	99	-0.27	6.66	-0.34
1980 07 08	PPT	1	42.78	7.29	7.26	118	-0.03	7.22	-0.07
1980 07 17	PPT	1	43.19	7.90	7.85	165	-0.05	7.62	-0.28
1981 07 06	PPT	1	36.59	7.41	6.84	91	-0.57	7.11	-0.30
1981 07 15	PPT	1	40.79	6.76	6.88	125	0.12	6.66	-0.10
1981 10 25	PPT	1	58.68	6.85	6.84	131	-0.01	6.77	-0.08
1982 06 07 A	PPT	1	61.04	6.46	6.46	97	0.00	6.57	0.11
1982 06 07 B	PPT	1	60.84	6.43	6.33	139	-0.10	6.38	-0.05
1982 08 05	PPT	1	43.16	6.51	6.74	130	0.23	6.49	-0.02
1982 12 19	PPT	1	25.39	7.30	7.28	116	-0.02	7.24	-0.06
1983 05 26	PPT	1	87.84	7.66	7.82	161	0.16	7.40	-0.26
1983 10 04	PPT	1	72.74	7.53	7.37	155	-0.16	7.23	-0.30
1984 02 07	PPT	1	48.97	7.40	7.43	115	0.03	7.51	0.11
1984 03 24	PPT	1	83.67	6.80	6.65	120	-0.15	6.52	-0.28
1985 03 03	PPT	1	70.32	8.01	7.75	96	-0.26	7.62	-0.39
1985 04 09	PPT	1	70.53	6.70	6.72	120	0.02	6.60	-0.10
1985 09 19	PPT	1	58.40	8.04	7.76	151	-0.28	7.66	-0.38
1985 09 21	PPT	1	58.87	7.40	7.38	161	-0.02	7.25	-0.15
1985 11 28 A	PPT	1	42.58	6.48	6.92	132	0.44	6.59	0.11
1985 11 28 B	PPT	1	42.64	6.56	6.69	132	0.13	6.78	0.22
1985 12 21	PPT	1	42.33	6.76	6.82	122	0.06	6.77	0.01
1986 04 30	PPT	1	58.18	6.49	6.51	131	0.02	6.41	-0.08
1986 05 07	PPT	1	72.38	8.02	7.99	168	-0.03	7.71	-0.31
1986 10 20	PPT	1	27.08	7.95	7.65	63	-0.30	7.51	-0.44
1987 02 08	PPT	1	62.16	7.05	7.18	104	0.13	6.92	-0.13
1987 03 05	PPT	1	73.50	7.39	7.42	121	0.03	7.30	-0.09
1987 03 06	PPT	1	75.33	6.80	6.86	129	0.06	6.84	0.04
1987 06 27	PPT	1	72.44	5.92	5.72	61	-0.20	5.79	-0.13
1987 07 06	PPT	1	41.06	5.98	6.49	104	0.51	6.07	0.09
1987 08 08	PPT	1	74.88	6.90	7.05	111	0.15	6.78	-0.12
1987 09 03	PPT	1	55.90	7.15	6.69	91	-0.46	7.17	0.02
1987 09 28 A	PPT	1	40.17	6.28	6.33	113	0.05	6.10	-0.18
1987 09 28 B	PPT	1	40.15	5.88	5.94	116	0.06	5.70	-0.18

distance corrections for Rayleigh waves are of course unchanged. In order to define suitable source corrections, it is necessary to restrict the depth range to intervals where the excitation E does not vary too much. Preliminary work shows that this is possible at very long periods in the two depth intervals 80–200 km and 400–670 km, where the most intense intermediate and deep seismicity takes place.

7. CONCLUSIONS

We have shown that spectral amplitude measurements of mantle Rayleigh waves can be converted to a magnitude scale, M_m, which is directly related to the seismic moment M_0 of the earthquake. The philosophy of a magnitude measurement, which uses the records of a single station and ignores the focal geometry and the exact depth of the source, can be used successfully to obtain a real-time estimate of the seismic moment. A study of more than 250 records shows that average residuals at typical stations are on the order of 0.1–0.2 magnitude units, and standard deviations are on the order of 0.2 . These numbers compare very favorably with the typical performance of classical magnitude scales, or even with the scatter in moment values published by individual investigators.

Furthermore, by letting the period at which the measurement is made vary and by keeping the largest resulting magnitude, we effectively guard against interference and saturation effects, which have plagued the standard magnitude scales, such as M_s, for 50 years. Only for a station sitting in an exact node of radiation in the case of a "pure" focal mechanism would our method be systematically inaccurate. Our experience shows that in such a geometry, multipathing effects can to some extent reduce the expected error; furthermore, the extension of the concept to Love waves should help guard against this problem.

In addition, we want to emphasize that (11) is, to our knowledge, the first magnitude scale in which all

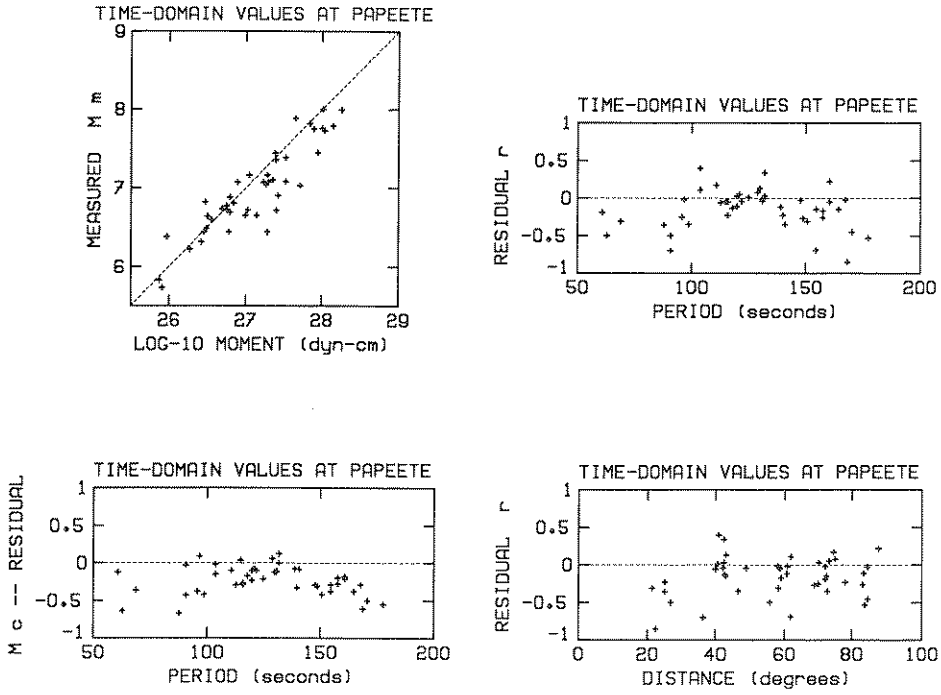

Fig. 16. Time-domain values of M_m^{TD} and population of residuals r^{TD} and r_c^{TD} plotted as a function of M_0, period, and distance for 42 earthquakes at Papeete.

oefficients and constants are fully justified on the basis of theoretical arguments. Therefore the present study is the first attempt to set the concept of magnitude on a firm theoretical basis.

By providing in real time, upon arrival of the Rayleigh wave train, an estimate of the seismic moment of the earthquake source, M_m has obviously a considerable potential for accurate tsunami warning. Since the method does not break down at very short distances, it is particularly valuable for the rapid evaluation of tsunami danger at regional distances, especially in sparsely populated areas where direct reports from the source region may not be available. Obvious examples are the Alaska-Aleutian arc and the whole Southwest Pacific region.

The calculations involved in the computations of M_m are extremely simple. They can easily be implemented on a personal computer and, as shown on Figure 17, lend themselves well to full automation [*Talandier et al.*, 1987; *Talandier and Okal*, 1989]. Even in the absence of such commonly available hardware the method has great potential: for any given seismic observatory, the regionalized distance corrections can be tabulated in advance for all epicentral areas bearing substantial tsunami risk. As an alternative, the average distance corrections C_D^{aver} listed in Table 7 can be used with negligible loss of accuracy. The time domain variant of the method can then be implemented with no more than a ruler, a pencil, and a hand-calculator.

Finally, we wish to conclude by illustrating the effectiveness of the method in tsunami warning: the seismic record shown on Figure 17 was used to evaluate tsunami potential immediately following the Aleutian earthquake of May 7, 1986. As a result of the estimate $M_m = 8.0$, no tsunami warning was issued for Polynesia. In contrast, a false alarm based largely on reported M_s values was issued for Oahu and along the Pacific Northwest coast of the U.S. mainland.

While the assessment of the relative dangers of failure to warn and false alarms is largely a philosophical and social task outside the responsibility of Earth scientists, it is clear that the scientific community has a duty to the public to provide swiftly the most accurate information possible on the parent earthquake and its tsunamigenic characteristics. We strongly believe that the use of the magnitude scale M_m is an important step in that direction.

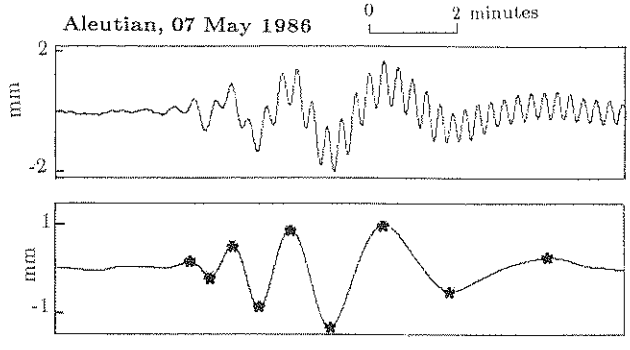

Fig. 17. Example of the use of M_m^{TD} in the automatic retrieval of the seismic moment of an earthquake. (Top) Broadband seismic record of the Aleutian earthquake (May 7, 1986) at Papeete. (Bottom) After filtering out the periods shorter than 40 s, the minima and maxima of the wave are automatically detected (asterisks), and the computation of the magnitude proceeds according to (19).

Acknowledgments. We are grateful to our Caltech colleagues for the use of the Pasadena archives. The PAS records were hand-digitized at Northwestern by Christina Lee. The maps on Figures 5–7 were produced using software developed by Paul Stoddard. We are grateful to Barbara Romanowicz for access to the GEOSCOPE data and for discussions of her results prior to publication. We thank John Woodhouse and Göran Ekström for updated tapes of the Harvard CMT data set. The paper benefited from careful reviews by Katsuyuki Abe and George Purcaru. Finally, we wish to pay tribute to the memory of Otto Nuttli, whose last discussion with one of us (E.A.O.) was about the potential of this new magnitude scale. This research has been supported by Commissariat à l'Energie Atomique (France), and the National Science Foundation, under grant EAR-87-20549.

REFERENCES

Abe, K., Mechanisms and tectonic implications of the 1966 and 1970 Peru earthquakes, *Phys. Earth Planet. Inter., 5,* 367-379, 1972.

Aki, K., Generation and propagation of *G* waves from the Niigata earthquake of June 16, 1964, part 2, Estimation of earthquake moment, released energy, and stress-strain drop from the *G* wave spectrum, *Bull. Earthquake Res. Inst. Univ. Tokyo, 44,* 73-88, 1966.

Aki, K., Scaling law of earthquake spectrum, *J. Geophys. Res., 72,* 1217-1231, 1967.

Aki, K., Scaling law of earthquake source-time function, *Geophys. J. R. Astr. Soc., 31,* 3-25, 1972.

Brune, J.N., and G.R. Engen, Excitation of mantle Love waves and definition of mantle wave magnitude, *Bull. Seismol. Soc. Am., 59,* 923-933, 1969.

Brune, J.N., and C.-Y. King, Excitation of mantle Rayleigh waves of period 100 s as a function of magnitude, *Bull. Seismol. Soc. Am., 57,* 1355-1365, 1967.

Canas, J., and B.J. Mitchell, Lateral variation of surface-wave anelastic attenuation across the Pacific, *Bull. Seismol. Soc. Am., 68,* 1637-1650, 1978.

Cifuentes, I.L., and P.G. Silver, Low-frequency characteristics of the great 1960 Chilean earthquake, *J. Geophys. Res., 94,* 643-663, 1989.

Dewey, J.W., and W. Spence, Seismic gaps and source zones of recent large earthquakes in coastal Peru, *Pure Appl. Geophys., 117,* 1148-1171, 1979.

Dziewonski, A.M., and D.L. Anderson, Preliminary reference Earth model, *Phys. Earth Planet. Inter., 25,* 297-356, 1981.

Dziewonski, A.M., A. Friedman, D. Giardini, and J.H. Woodhouse, Global seismicity of 1982: Centroid moment tensor solutions for 308 earthquakes, *Phys. Earth Planet. Inter., 33,* 76-90, 1983*a*.

Dziewonski, A.M., A. Friedman, and J.H. Woodhouse, Centroid moment-tensor solutions for January–March 1983, *Phys. Earth Planet. Inter., 33,* 71-75, 1983*b*.

Dziewonski, A.M., J.E. Franzen, and J.H. Woodhouse, Centroid moment-tensor solutions for April–June 1983, *Phys. Earth Planet. Inter., 33,* 243-249, 1983*c*.

Dziewonski, A.M., J.E. Franzen, and J.H. Woodhouse, Centroid moment-tensor solutions for October–December 1983, *Phys. Earth Planet. Inter., 34,* 129-136, 1984*a*.

Dziewonski, A.M., J.E. Franzen, and J.H. Woodhouse, Centroid moment-tensor solutions for January–March 1984, *Phys. Earth Planet. Inter., 34,* 209-219, 1984*b*.

Dziewonski, A.M., J.E. Franzen, and J.H. Woodhouse, Centroid moment-tensor solutions for April–June 1984, *Phys. Earth Planet. Inter., 37,* 87-96, 1985*a*.

Dziewonski, A.M., J.E. Franzen, and J.H. Woodhouse, Centroid moment-tensor solutions for July–September 1984, *Phys. Earth Planet. Inter., 38,* 203-213, 1985*b*.

Dziewonski, A.M., J.E. Franzen, and J.H. Woodhouse, Centroid moment-tensor solutions for October–December 1984, *Phys. Earth Planet. Inter., 39,* 147-156, 1985*c*.

Dziewonski, A.M., J.E. Franzen, and J.H. Woodhouse, Centroid moment-tensor solutions for January–March 1985, *Phys. Earth Planet. Inter., 40,* 249-258, 1985*d*.

Dziewonski, A.M., J.E. Franzen, and J.H. Woodhouse, Centroid moment-tensor solutions for April–June 1985, *Phys. Earth Planet. Inter., 41,* 215-224, 1986*a*.

Dziewonski, A.M., J.E. Franzen, and J.H. Woodhouse, Centroid moment-tensor solutions for July–September 1985, *Phys. Earth Planet. Inter., 42,* 205-214, 1986*b*.

Dziewonski, A.M., J.E. Franzen, and J.H. Woodhouse, Centroid moment-tensor solutions for October–December 1985, *Phys. Earth Planet. Inter., 43,* 185-195, 1986*c*.

Dziewonski, A.M., G. Ekström, J.E. Franzen, and J.H. Woodhouse, Global seismicity of 1977; Centroid moment tensor solutions for 471 earthquakes, *Phys. Earth Planet. Inter., 45,* 11-36, 1987*a*.

Dziewonski, A.M., G. Ekström, J.E. Franzen, and J.H. Woodhouse, Global seismicity of 1978; Centroid moment tensor solutions for 512 earthquakes, *Phys. Earth Planet. Inter., 46,* 316-342, 1987*b*.

Dziewonski, A.M., G. Ekström, J.E. Franzen, and J.H. Woodhouse, Global seismicity of 1979; Centroid moment tensor solutions for 524 earthquakes, *Phys. Earth Planet. Inter., 48,* 18-46, 1987*c*.

Dziewonski, A.M., J.E. Franzen, and J.H. Woodhouse, Centroid moment-tensor solutions for January–March 1986, *Phys. Earth Planet. Inter., 45,* 1-10, 1987*d*.

Dziewonski, A.M., G. Ekström, J.E. Franzen, and J.H. Woodhouse, Centroid moment-tensor solutions for April–June 1986, *Phys. Earth Planet. Inter., 45,* 229-239, 1987*e*.

Dziewonski, A.M., G. Ekström, J.E. Franzen, and J.H. Woodhouse, Centroid moment-tensor solutions for July–September 1986, *Phys. Earth Planet. Inter., 46,* 305-315, 1987*f*.

Dziewonski, A.M., G. Ekström, J.H. Woodhouse, and G. Zwart, Centroid moment-tensor solutions for October–December 1986, *Phys. Earth Planet. Inter., 48,* 5-17, 1987*g*.

Dziewonski, A.M., G. Ekström, J.E. Franzen, and J.H. Woodhouse, Global seismicity of 1980; Centroid moment tensor solutions for 515 earthquakes, *Phys. Earth Planet. Inter., 50,* 127-154, 1988*a*.

Dziewonski, A.M., G. Ekström, J.E. Franzen, and J.H. Woodhouse, Global seismicity of 1981; Centroid moment tensor solutions for 542 earthquakes, *Phys. Earth Planet. Inter., 50,* 155-182, 1988*b*.

Dziewonski, A.M., G. Ekström, J.H. Woodhouse, and G. Zwart, Centroid moment-tensor solutions for January–March 1987, *Phys. Earth Planet. Inter., 50,* 116-126, 1988*c*.

Dziewonski, A.M., G. Ekström, J.H. Woodhouse, and G. Zwart, Centroid moment-tensor solutions for April–June 1987, *Phys. Earth Planet. Inter., 50,* 215-225, 1988*d*.

Dziewonski, A.M., G. Ekström, J.H. Woodhouse, and G. Zwart, Centroid moment-tensor solutions for July–September 1987, *Phys. Earth Planet. Inter., 53,* 1-11, 1988*e*.

Ekström, G., and A.M. Dziewonski, Evidence of bias in estimations of earthquake size, *Nature, 332,* 319-323, 1988.

Geller, R.J., Scaling relations for earthquake source parameters and magnitudes, *Bull. Seismol. Soc. Am., 66,* 1501-1523, 1976.

Geller, R.J., Part I. Earthquake source models, magnitudes and scaling relations. Part II. Amplitudes of rotationally split normal modes for the 1960 Chilean and 1964 Alaskan earthquakes, Ph.D. dissertation, 211 pp., Calif. Inst. of Technol., Pasadena, 1977.

Gilman, R., Report on some experimental long-period systems, *Bull. Seismol. Soc. Am., 50,* 553-559, 1960.

Gutenberg, B., The energy of earthquakes, *Quat. J. Geol. Soc. London, 112,* 1-14, 1956.

Gutenberg, B., and C.F. Richter, On seismic waves (third paper), *Gerlands Beitr. Geophys., 47,* 73-131, 1936.

Hwang, H.-J., and B.J. Mitchell, Shear velocities, Q_β, and the frequency dependence of Q_β in stable and tectonically active regions from surface wave observations, *Geophys. J. R. Astr. Soc., 90,* 575-613, 1987.

Jordan, T.H., Global tectonic regionalization for seismological data analysis, *Bull. Seismol. Soc. Am., 71,* 1131-1141, 1981.

Kanamori, H., The Alaska earthquake of 1964: Radiation of long-period surface waves and source mechanism, *J. Geophys. Res., 75,* 5029-5040, 1970.

Kanamori, H., The energy release in great earthquakes, *J. Geophys. Res., 82,* 2981-2987, 1977.

Kanamori, H., and J.J. Cipar, Focal process of the great Chilean earthquake, May 22, 1960, *Phys. Earth Planet. Inter., 9,* 128-136, 1974.

Kanamori, H., and G.S. Stewart, Mode of strain release along the Gibbs Fracture Zone, Mid-Atlantic Ridge, *Phys. Earth Planet. Inter., 11,* 312-332, 1976.

Lay, T., and H. Kanamori, Earthquake doublets in the Solomon Islands, *Phys. Earth Planet. Inter., 21,* 283-304, 1980.

Lundgren, P.R., and E.A. Okal, Source processes of 'anomalous' subduction zone earthquakes in the Southwest Pacific (abstract), *Seismol. Res. Lett., 59,* 37, 1988.

Mitchell, B.J., and G.-K. Yu, Surface-wave dispersion, regionalized velocity models, and anisotropy of the Pacific crust and upper mantle, *Geophys. J. R. Astr. Soc., 63,* 497-514, 1980.

Monfret, T., and B.A. Romanowicz, Importance of on-scale observations of first-arriving wave trains for source studies: example of the Chilean event of March 3, 1985 observed on GEOSCOPE and IDA networks, *Geophys. Res. Lett., 13,* 1015-1018, 1986.

Nakanishi, I., Shear velocity and shear attenuation models inverted from the world-wide and pure-path average data of mantle Rayleigh waves ($_0S_{25}$ to $_0S_{80}$) and fundamental normal modes ($_0S_2$ to $_0S_{24}$), *Geophys. J. R. Astr. Soc., 66,* 83-130, 1981.

Okal, E.A., The effect of intrinsic oceanic upper-mantle heterogeneity on the regionalization of long-period Rayleigh wave phase velocities, *Geophys. J. R. Astr. Soc., 49,* 357-370, 1977.

Okal, E.A., Seismic parameters controlling far-field tsunami amplitudes: A review, *Nat. Hazards J., 1,* 67-96, 1988.

Okal, E.A., A theoretical discussion of time domain magnitudes: The Prague formula for M_s and the mantle magnitude M_m, *J. Geophys. Res.,* this issue, 1989.

Okal, E.A., and R.J. Geller, On the observability of isotropic seismic sources: The July 31, 1970 Colombian earthquake, *Phys. Earth Planet. Inter., 18,* 176-196, 1979.

Okal, E.A., and J. Talandier, M_m: Theory of a variable-period mantle magnitude, *Geophys. Res. Lett., 14,* 836-839, 1987.

Purcaru, G., and H. Berckhemer, A magnitude scale for very large earthquakes, *Tectonophysics, 49,* 189-198, 1978.

Purcaru, G., and H. Berckhemer, Quantitative relations of seismic source parameters and a classification of earthquakes, *Tectonophysics, 84,* 57-128, 1982.

Romanowicz, B., M. Cara, J.-F. Fels, and D. Rouland, GEOSCOPE: A French initiative in long-period three-component global seismic networks, *Eos, Trans. AGU, 65,* 753-754, 1984.

Richter, C.F., An instrumental earthquake magnitude scale, *Bull. Seismol. Soc. Am., 25,* 1-32, 1935.

Shimazaki, K., Nemuro-Oki earthquake of June 17, 1973: A lithospheric rebound at the upper half of the interface, *Phys. Earth Planet. Inter., 9,* 314-327, 1974.

Stewart, G.S., and S.N. Cohn, The 1976 August 16, Mindanao, Philippine earthquake (M_s = 7.8) — Evidence for a subduction zone South of Mindanao, *Geophys. J. R. Astr. Soc., 57,* 51-65, 1979.

Talandier, J., and E.A. Okal, An algorithm for automated tsunami warning in French Polynesia, based on mantle magnitudes, *Bull. Seismol. Soc. Amer., 79,* in press, 1989.

Talandier, J., D. Reymond, and E.A. Okal, M_m: Use of a variable-period mantle magnitude for the rapid one-station estimation of teleseismic moments, *Geophys. Res. Lett., 14,* 840-843, 1987.

Vaněk, J., A. Zátopek, V. Kárník, N.V. Kondorskaya, Yu. V. Riznichenko, E.F. Savarenskii, S.L. Solov'ev, and N.V. Shebalin, Standardization of magnitude scales, *Izv. Akad. Nauk SSSR, Ser. Geofiz., 2,* 153-158, 1962.

Wieland, E., and G. Streckeisen, The leaf-spring seismometer: design and performance, *Bull. Seismol. Soc. Am., 72,* 2349-2367, 1982.

Williams, B.R., M_0 calculations from a generalized *AR* parameter method for WWSSN instruments, *Bull. Seismol. Soc. Am., 69,* 329-351, 1979.

Woodhouse, J.H., and A.M. Dziewonski, Mapping the upper mantle: Three-dimensional modeling of Earth structure by inversion of seismic waveforms, *J. Geophys. Res., 89,* 5953-5986, 1984.

E.A. Okal, Department of Geological Sciences, Northwestern University, Evanston, Illinois 60208.

J. Talandier, Laboratoire de Géophysique, Commissariat à l'Energie Atomique, Boîte Postale 640, Papeete, Tahiti, French Polynesia.

(Received June 1, 1988;
revised October 20, 1988;
accepted November 2, 1988.)